Paper I

"Development, implementation and verification of a physics-based Si/SiGe HBT model for millimeter-wave non-linear circuit simulations"

S. Bruce, A. Rydberg, H. Schumacher, U. Erben, J-F. Luy, M. Karlsteen and M. Willander

Proceedings of the 26th European Microwave Conference, Prague, Czech Republic, 1996, vol. 2, pp. 903–905

Development, implementation and verification of a physics-based Si/SiGe HBT model for millimeter-wave non-linear circuit simulations.

S. Bruce, A. Rydberg*,
H. Schumacher, U. Erben**,
J-F. Luy***,
M. Karlsteen, M. Willander****.

*Circuits and Systems Group,
Department of Technology,
University of Uppsala, Box 534,
S-751 21 Uppsala, Sweden

**Department of Electron Devices and Circuits,
University of Ulm, D-89069 Ulm, Germany

***Daimler-Benz Research Center,
P. O. Box 2360, D-89081 Ulm, Germany

****Linköping Institute of Technology,
Department of Physics and Measurements
Technology, S-581 83 Linköping, Sweden

Abstract

A physics-based large-signal model including thermal dependence has been developed for Si/SiGe HBTs. The model takes into account several effects that are important for the operation of Si/SiGe HBTs and is directly related to the parameters in the fabrication process. Using extraction procedures for only a few parameters that inherently are difficult to predict, either due to uncertainties in the fabrication process or due to complex physical relations, a good agreement is found between the model and measurements. The model has been implemented using a commercial CAD-system facilitating design of non-linear Si/SiGe HBT applications. Thus the model has been used to design and predict the behaviour of a doubler circuit operating at 55 GHz with good accuracy.

Introduction

The recent progress in SiGe technology which has yielded HBTs with f_{max} of 160 GHz [1], making it possible to design circuits for the important frequency range used in automotive applications. For analysis and implementation of Si/SiGe HBTs in non-linear microwave applications, the access to an accurate physics-based large-signal model with parameters directly related to the fabrication process and describing the physical properties of SiGe is of great importance. The thermal properties of the Si/SiGe HBT which plays an important part in power applications has also to be taken into account in a model. Such model has been developed and it is now used for the design and optimization of Si/SiGe HBT millimeter-wave frequency doublers operating at 55 GHz.

Model

A modified Ebers-Moll model, having transit time delay added to the current generator, can be shown to sufficiently model HBT transistors at microwave frequencies [2]. The model has the benefit of taking into account the physical properties of the transistor and of having only a moderate amount of components. Also of importance is that variation of the technological parameters can be accounted for.

The implementation of the model has been done in a SPICE-like simulator using MDS from Hewlett Packard. A special feature called SDD (Symbolically Defined Device) has been used for modelling the intrinsic part of the transistor (the shaded part in Fig. 1a shows a schematic of the modelling). Embedding the intrisic part is a shell composed of lumped circuit elements which accounts for the extrinsic transistor (elements outside shaded part in Fig. 1a) and also for pad parasitics.

By utilizing the ability to control the current inside the SDD via equations, it is possible to mathematically create a discrete analogy to the processes occuring. Thanks to this, the ideal electron and hole injection currents in each junction are treated separately which makes the modelling of the heterojunctions straight-forward. Furthermore, the common base amplification factor can be decomposed. The factors α_F and α_R no longer need to account for the emitter injection efficiency, but only for base transport factor and a possible bulk breakdown in the space charge regions.

The current generators I_{LCB} and I_{LBE} have been added to empirically model high injection effects and the surface currents occurring on a mesa device structure. The capacitances C_{BE} and C_{BC} have been calculated using the SPICE model for junction depletion capacitances taking into account charge compensation in the collector space charge region which occurs at high collector currents for the base-collector capacitance C_{BC} [3].

Thermal modelling has been accomplished by creating a versatile interface via the SDD. Thanks to this, it is possible to use different complexities in the thermal model; from a lumped thermal resistance to non-linear models derived from FEM-simulations, see Fig 1b.

Parameter Extraction and Verification of Model

The analytical expressions which the model parameters are based on are useful for a first estimation of transistor behaviour. Starting values for the parameters are calculated from given device geometries, layer structure and known semiconductor properties. Due to the complexity in the physical relations governing the semiconductor and to uncertainties in the fabrication process, some of these parameters that are used in the calculations inherently contain errors. Measurements are therefore needed to adjust certain parameters and to verify the accuracy of the calculations.

The measurements, performed at a known ambient temperature, result in Gummel, I-V-plots and S-parameter curves at different bias. Desirable is to measure the S-parameters at low and high I_C and at least one intermediate value to get information of transistor behaviour at the most important bias levels.

The fitting of parameters is then done in a two-step process where initially only the technological parameters are allowed to vary within limits known from the fabrication process. Following this, elements in the equivalent circuit that do not directly relate to the intrinsic transistor are varied to further improve the accuracy.In order to verify the model, parameters fora $1\mu m \times 20\mu m$ emitter-area HBT with device geometry and layer structure described in ref. [4] were calculated and further tuned for accuracy using the approach described above.

Using the same analytical expressions that were used for calculating the model parameters, the IV-characteristics and S-parameters are also simulated, see Fig. 2 and 3. As can be seen in Fig. 2 and 3, the simulated results agree with both the DC and RF measurements. The slightly sharper kink for simulated IV-characteristics in Fig. 2 at low V_{CE} and high I_C compared to the measured data is likely caused by the Kirk-effect [5]. The typical decrease in β at high I_C with increasing V_{CE} is caused by the self heating effect [3].

The model has also been used to design an active frequency doubler [6] and a comparison between measured and simulated data for this component can be seen in Fig. 4. The doubler is operating at a frequency of 55 GHz. This is a higher frequency than the transistor has been characterised to. Still, the extrapolated data show good agreement with measurements.

Conclusions

We have presented a physics-based large-signal Si/SiGe HBT model which uses data given from the fabrication process for finding the model parameters. With fitting of a few parameters it is possible to accurately model the large signal behavior up to millimeterwave frequencies.

Acknowledgement

The authors wishes to thank U. Spitzberg for help with measurements, M. Birk and R. Schnitzer for technical assistance, J. Schneider for useful discussions, K.M. Strohm for continuous technological support, H. Kibbel for layer growth, A. Schüppen and A. Gruhle for essential comments regarding the HBT process and D. Eisbrenner for technical support. The Swedish Board for Industrial and Technological Development (NUTEK) and the ISS90 foundation are acknowledged for financial support.

References

[1]: A. Schüppen, U. Erben, A. Gruhle, H. Kibbel, H. Schumacher, and U. König, "Enhanced SiGe Heterojunction Bipolar Transistors with 160 GHz-f_{max}," IEEE Intl. Electron Devices Meeting (IEDM 95) Tech. Dig., pp. 30.4.1-30.4.4, 1995.

[2] D. A. Teeter, J. R. East, R. K. Mains, and G. I. Haddad, "Large-signal numerical and analytical HBT models," IEEE Trans. Electron Devices, vol. 40, no. 5, pp. 837-845, May 1993.

[3] Q. M. Zhang, J. Hu, J. Sitch, R. K. Surridge, and J. M. Xu, "A new large signal HBT model," in 1994 IEEE MTT-S Int. Microwave Symp. Dig., San Diego, California, May 1994, pp 1253-1256.

[4] A. Gruhle, H. Kibbel, U. König, U. Erben, and E. Kasper, "MBE-grown Si/SiGe HBTs with high β, ft, and fmax," IEEE Electron Device. Lett., vol. 13, pp 206-208, 1992.

[5] S. M. Sze, "Physics of semiconductor devices," 2nd ed., p. 145, John Wiley and Sons, 1981.

[6] S. Bruce, M. Kim, A. Rydberg, K. M. Strohm, and F. Beiβwanger, "On the design of a 55 GHz Si/SiGe HBT frequency doubler operating close to F_{max}," submitted for presentation at EuMC, Prague, Czech Republic, 1996.

FIGURES

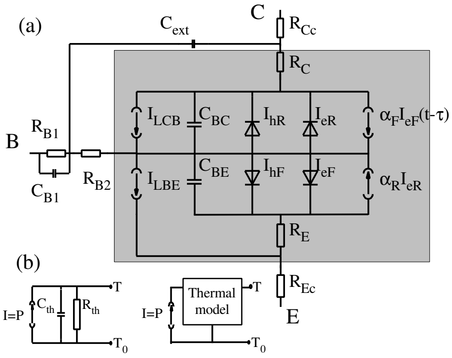

Fig. 1. Large signal HBT model: (a) electrical model, (b) examples of thermal equivalents for the circuit.

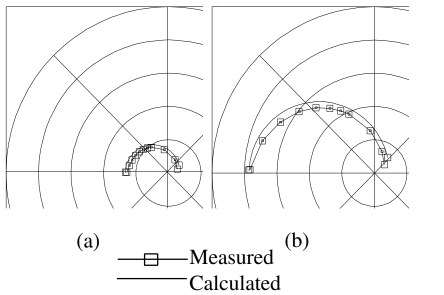

Fig. 3. Measured and simulated S_{21} from 45 MHz to 50 GHz. DC-bias is 3V, 1mA (a) and 3V, 10mA (b). Full scale of the plot is 10.

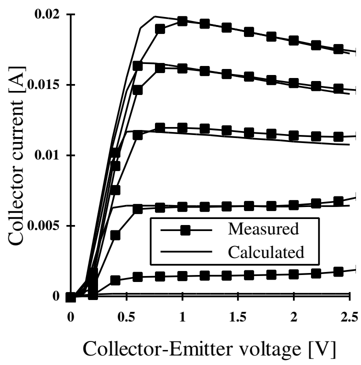

Fig. 2. Measured and calculated I-V characteristics varying I_B from 50 to 250 μA.

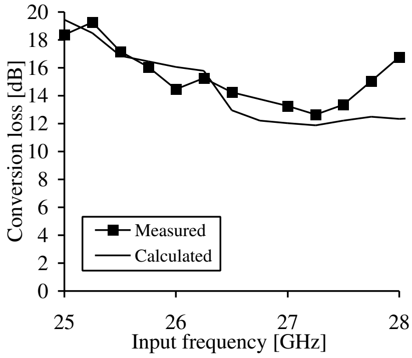

Fig. 4. Conversion loss for an active frequency multiplier.

Paper II

"On the design of a 55 GHz Si/SiGe HBT frequency doubler operating close to f_{max}"

S. Bruce, M. Kim, A. Rydberg,
K. M. Strohm and F. Beißwanger

Proceedings of the 26th European Microwave Conference, Prague, Czech Republic, 1996, vol. 1, pp. 297–299.

On the design of a 55 GHz Si/SiGe HBT frequency doubler operating close to f_{max}

S. Bruce, M. Kim*,
A. Rydberg,
K. M. Strohm, F. Beiβwanger**

Circuits and Systems Group,
Department of Technology,
Uppsala University, Box 534,
S-751 21 Uppsala, Sweden.

*MS 168-314, Jet Propulsion Laboratory,
4800 Oak Grove Dr.,
Pasadena CA 91109, U.S.A.

**Daimler Benz Research Centre,
P.O. Box 2360, D-89013 Ulm, Germany.

Abstract

In this paper we present for the first time experimental results on a frequency doubler using a Si/SiGe HBT as the non-linear element. Despite the high output operating frequency being close to f_{max}, 67 GHz, for the Si/SiGe HBT, the conversion efficiency in a not completely optimised circuit was found to be better than -12 dB. The 3 dB bandwidth for the doubler was about 7.4%. These results are found to be comparable to an HFET doubler operating equally close to its f_{max}. The results agree well with the prediction for the multiplier from a developed physics-based large-signal HBT model. Prediction by the model using harmonic balance simulation at 55 GHz shows that a conversion efficiency for the Si/SiGe HBT of about 5 dB can be expected from future optimised circuits.

Introduction

Silicon based active devices such as Si/SiGe Heterojunction Bipolar Transistors (HBT) have shown to have great potentials of performance where devices with a maximum frequency of oscillation (f_{max}) of 80 GHz have been implemented in circuits [1] and f_{max} of 160 GHz has been reached recently in common emitter configuration for single devices [2]. Thus f_{max} for state of the art Si/SiGe HBTs are well above the important operating frequencies to be used in automotive applications such as car - car communication and car radar. In order to evaluate the feasibility of this technology for applications at millimeterwave frequencies, an active second harmonic 55 GHz frequency doubler using an Si/SiGe HBT as the active device has been designed.

Design of the Doubler

The circuit structure used in the implementation of the doubler has been chosen to be Coplanar Waveguide (CPW) due to the large impedance range and lower dispersion that can be achieved for this circuit technology compared to microstrip and also due to the practical advantage of not having to use viaholes for ground connection. This is of particular importance in the case of monolithic integration of circuits [3]. The monolithic matching circuits for the multiplier, implemented on high-ohmic silicon, have been centred around 50 ohm transmission-lines in order to reduce the complexity in the number of circuits needed to design the doubler.

To ensure a good understanding on how to realise the passive structures, consisting of shorts, opens, crosses and MIM-capacitors, test circuits have been designed using E-M-field simulators from Hewlett Packard [4] and then fabricated. Results from measurements on the passive structures conform well with simulated data up to at least 40 GHz (current limit of the used measurement equipment). For the doubler circuit itself, the HBT was bonded into the monolithic passive circuitry using preformed beamleads, included in the electrical design. The layout of the 55 GHz doubler is shown in Fig.1. The input and output matching to 50 ohms were achieved using stub circuits where the stubs were terminated in shorts (MIM-capacitors). On the output, a filter (consisting of open quarter-wave stubs) was used to suppress the fundamental frequency.

A new physics-based large-signal Si/SiGe HBT model has been derived and used in the design of the frequency doubler. It employs a modified Ebers-Moll model which has technological data as input parameters. The heterojunction is accounted for by treating the different kinds of injections separately, which simplifies modelling of for example the current dependency of β.

With the use of fitting of given input parameters, within realistic limits, to measurements such as Gummel- and IV-plots in conjunction with S-parameters at different bias points, it is possible to model the transistors behaviour throughout the interesting region of operation with sufficient accuracy.

Measurements and Discussion

The measurement set-up for the evaluation of the fabricated doubler comprised of a HP8510C vector network analyser for S-parameter measurements. A synthesised sweeper together with a power amplifier was used for the power measurements. The circuit was contacted on input and output side using coplanar probes. The output power was measured using a waveguide V-band power-sensor in order to further suppress the fundamental frequency, being below the cut-off frequency of the waveguide.

The measured frequency doubler showed a conversion efficiency of better than -12 dB at an input power of 1.2 dBm and a DC-bias of 4 V and 3 mA, see Fig. 2. These results are found to be comparable to an HFET doubler operating equally close to its f_{max} [5]. The 3 dB power-bandwidth for the multiplier was measured to be about

7.4%, see Fig 3. In Fig. 3 is also shown the calculated conversion efficiency for the doubler using the derived HBT-model and the calculated impedances for the input and output embedding circuits. The good agreement between theory and experiments makes it possible to predict the conversion behaviour for different HBT devices and improving the design of the doubler.

The multiplier was originally designed for a Si/SiGe HBT (here called DT9502) having a different doping profile, thus having somewhat different S-parameters compared to the used device (here called 3147A1) which was available at the time of implementation. The difference in S-parameters between the devices implied that the used device (3147A1) is not optimally matched for working in this frequency multiplier. The effect of this difference in transistor behaviour can be seen in Fig. 3 where the doubler structure has been simulated using both the DT9502 and 3147A1 as active device.

Preliminary Harmonic-Balance simulations with the new transistor show that a conversion gain of about 5 dB can be expected if optimised matching circuits are employed.

Conclusion

A frequency doubler for 55 GHz with a conversion efficiency of better than -12 dB operating at an output frequency near f_{max} for the device has been designed. By improving the matching circuits to the transistor, an enhancement in conversion of upto 17 dB can be expected. This does not put any demands on improved performance of the transistor itself.

Acknowledgements

We would like to acknowledge Dr. J.-F. Luy and Dr. F. Schäffler at Daimler Benz Research Centre for helpful discussions. We also acknowledge Dr. H. Zirath, Chalmers Inst. of Tech., Göteborg, Sweden, and Dr. Biebl, Tech. Univ. of Munich, Germany, for help with instrumentation. The Hewlett Packard is acknowledged for donating the CAD-systems used in the simulations. The Swedish National Board for Industrial and Technical Development (NUTEK) is acknowledged for financial support.

References

[1]: A. Gruhle, A. Schüppen, U. König , U. Erben, and H. Schumacher, “Monolithic 26GHz and 40GHz VCOs with SiGe Heterojunction Bipolar Transistors,” IEEE Intl. Electron Devices Meeting (IEDM) Tech. Dig., pp. 29.6.1-29.6.4, 1995.

[2]: A. Schüppen, U. Erben, A. Gruhle, H. Kibbel, H. Schumacher, and U. König, “Enhanced SiGe Heterojunction Bipolar Transistors with 160 GHz-f_{max},” IEEE Intl. Electron Devices Meeting (IEDM 95) Tech. Dig., pp. 30.4.1-30.4.4, 1995.

[3]: T. Itoh, "Overview of quasi-planar transmission lines," IEEE Trans. Microwave Theory Tech., vol. MTT-37, pp. 275-280, 1989.

[4]: High Frequency Structure Simulator (HFSS) and Momentum from Hewlett Packard, Santa Rosa System Division, Santa Rosa, CA, USA.

[5]: H. Zirath, I. Angelov, N. Rorsman, C. Karlsson, and E. Kollberg, “A balanced W-band HFET doubler,” Proc. 23rd European Microwave Conf., pp. 837-839, Madrid, 1993.

FIGURES

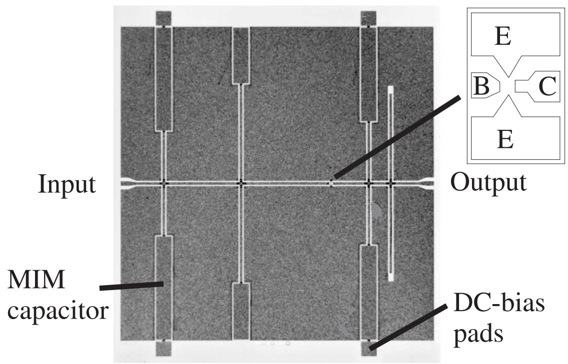

Fig. 1. The fabricated circuit. A schematic of the transistor is shown on the right.

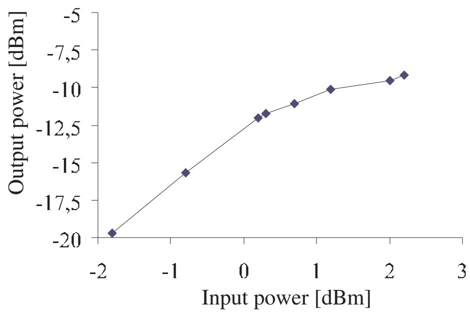

Fig. 2. Measured output power at 54.5 GHz versus source power at the fundamental frequency for the doubler circuit.

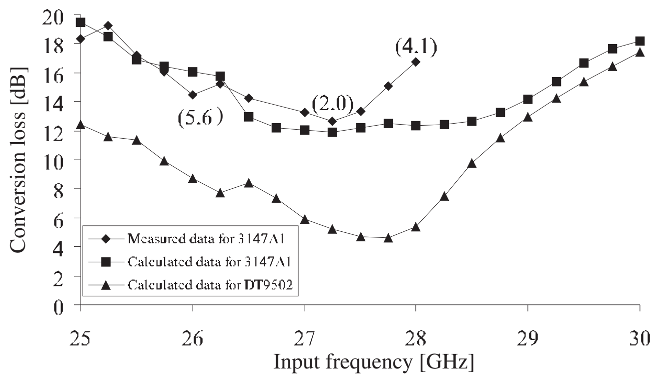

Fig. 3. Conversion loss versus frequency for the doubler circuit. Numbers within parenthesis depict source power at the input

Paper III

"Extraction of thermal time constant in HBTs using small signal measurements"

S. Bruce, A. Trasser, M. Birk,
A. Rydberg and H. Schumacher

Electronics Letters, vol. 33,
pp. 165 – 167, 1997.

Extraction of thermal time constant in HBTs using small signal measurements.

S. Bruce*, A. Trasser+, M. Birk+, A. Rydberg* and H. Schumacher+.
*Uppsala University, Box 534, S-751 21 Uppsala, Sweden.
+University of Ulm, Abt. EBS, D-89069 Ulm, Germany.

Abstract

A novel method for finding the thermal time constant of HBTs is proposed. It utilizes small signal measurements in the frequency domain of the typical negative differential resistance found in the active region, i.e., normal bias conditions for the device. In this way, non-linearities in the thermal resistivity does not disturb the extraction and the device needs only to be characterized in one bias point.

Introduction

Different methods for finding the thermal time constant of two terminal devices have been proposed[1][2][3], but to the authors knowledge so far none has been suggested which operates in the frequency domain. Furthermore, conventional extraction procedures need to achieve a strong variation of power dissipation during the extraction. The device needs to be operated under two different bias conditions: at low power dissipation (cold state) and at high power dissipation (hot state). This means that essential parameters need to be known over a wide range compared to small signal operation. The suggested approach does not suffer from these shortcomings.

Theoretical background and description of method

The proposed method utilizes the variation of HBT current gain with temperature. In a first approximation, the thermally dependent part of the common emitter current gain (β) for an HBT can be expressed by an exponential term:

$$\beta_{HBT} = \beta_0 * e^{\frac{\Delta E_g}{k_B T}} \qquad (1)$$

where T is the junction temperature and ΔE_g is the bandgap energy difference between emitter and base, assuming this is located in the valence band (for an NPN-type transistor). This is true for a graded base GaAs HBT or for SiGe HBTs with strained base layers. Due to the thermal dependence in eq. 1, HBTs will exhibit a negative differential resistance in the (active, non-saturated) region of an IV-curve since the internal power dissipation will heat the device. This can be seen in Fig. 1 (a) as the negative slope at collector-emitter voltages above approximately 1 V. The device has then been simulated in a steady-state, i.e., each bias point has been held for a much longer time than the thermal time constant (τ_T) and the junction has thus reached a stable temperature.

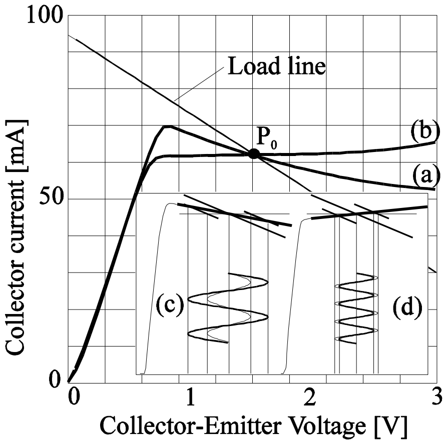

Fig. 1 Collector current versus collector-emitter voltage at a fixed base current. Employing thermal dependence (a), assuming a fixed junction temperature (b). A load line for a resistor in series with the collector is also shown. The inset shows schematically how the amplification of small signal input, v_{CC}, varies with frequency. Inset: (c) at low frequencies, the slope of the load line very closely resembles the slope of the IV-curve and thus creates an amplification of v_{CC}. (d) at high frequencies, the slope of the IV-curve has changed to become positive and v_{CC} is therefore attenuated. The thick curve is the small signal output, v_C, and the thin curve (equal in the two cases) is v_{CC}.

If the same sweep is done in a much shorter time ($<<\tau_T$), it means that the transient power dissipation within the device is not sufficient to alter the junction temperature and β will thus essentially remain constant which can be seen as a negligible or even a positive slope (caused by e.g. the Kirk-effect and Early-effect) in the IV-curve (see Fig. 1 (b)). By varying the bias point with a sine wave around a fixed power dissipation point (e.g. P_0 in Fig. 1), it is possible to find the transition between steady-state and transient mode and thus also the thermal time constant.

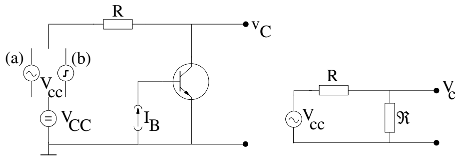

Fig. 2 Schematic of the measurement setup. On the left side the large signal setup with a constant base current (I_B) and a modulated collector voltage (V_{CC}+v_{cc}). In the frequency domain, v_{cc} is a sine wave (a). In the time domain (for later verification), v_{cc} is a voltage step (b). On the right side is a small signal equivalent where the transistor has been replaced by a frequency dependent resistor.

In the discussion below, signals will be defined in the following way: upper-case letters for signal type (i.e., V or I) denote time-independent magnitude and lower-case letters denote time dependence. Upper-case index denote complete part of signal and lower-case letters denote the modulating part. As an example, the complete signal v_C is then defined as $V_C+V_c\sin(\omega t)$ where V_C is the DC-part and $V_c\sin(\omega t)=v_c$ is the AC modulating part.

The circuit used for the measurements described above can be seen in Fig. 2. A DC voltage source (V_{CC}) is connected via a resistor (R) to the collector of the transistor and a constant current source (I_B) is connected to the base. By choosing appropriate values for I_B and V_{CC}, a bias point in the active region is found (e.g. P_0 in Fig. 1, the load line is the one of R). Around this point, the collector-emitter voltage is varied by modulating V_{CC} with a signal v_{cc}. Since this is a small signal operation, it suffices to study the small signal equivalent circuit, see Fig. 2, where the transistor has been substituted with a frequency dependent differential resistance ($\Re(f)$). Using ordinary voltage division the magnitude of v_c, V_c, is found as:

$$V_c = V_{cc} * \frac{\Re(f)}{R + \Re(f)} \qquad (2)$$

Since $\Re(f)$ can be negative, V_c can be greater than V_{cc}. At low frequencies this is the case and a schematic describing this process can be seen in Fig. 1(c). When modulating with higher frequencies, the signal changes in shorter times than τ_T and the junction temperature stays essentially constant. There is thus no longer a thermally induced negative differential resistance and the electronically induced positive differential resistance prevails, instead attenuating the signal, see schematic in Fig. 1 (d). Plotting V_c versus frequency in a Bode diagram, see Fig. 3, allows extraction of τ_T from the higher characteristic frequency by finding its 3 dB-point, assuming the device has no other time constants in the same order of magnitude as the one of τ_T.

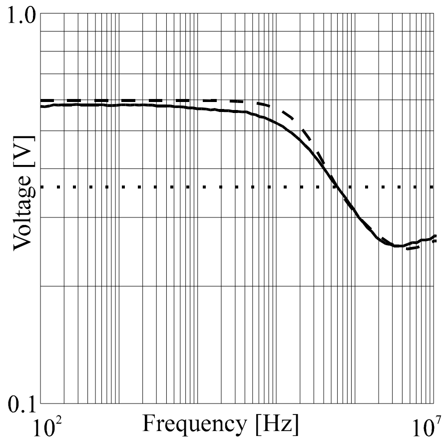

Fig. 3 Bode diagram of measured (full line) and calculated (dashed line) output signal magnitude,V_C, versus frequency. Low frequencies denote the steady state mode and high frequencies denote the transient mode. The dotted straight line corresponds to amplitude of fed small signal amplitude (V_{cc} in Fig. 2).

To achieve higher accuracy, an electrothermal model of the device can be used. Such a model has been developed and shown to accurately model SiGe HBTs from DC upto millimetre-wave frequencies [4]. It uses a modified Ebers-Moll model where the different physical processes occuring in the device are as closesly as possible modelled with lumped elements. Electron and hole injection are here treated separately using different diodes which gives an

efficient way of modelling the temperature dependence of β.
To model junction heating from internal power dissipation, an RC-network has been used in the model [4] where current and voltage drop has been related to internal power dissipation and device heating respectively. A thermal resistance (R_T) relates to the steady-state part and a thermal capacitance (C_T) relates to the transient part of the device heating. Together, these two parts define τ_T. The thermal resistance can be found either by direct extraction [5] or by fitting to a measured IV-curve. Using the electrothermal model in a setup like in Fig. 2, it is possible to fit C_T to the measured curve and from this calculate τ_T. The Harmonic Balance simulation method was chosen in order to have the same signal levels as in the measurement and thus facilitate the fitting procedure.

Measurements and verification

To verify the validity of this method, Si/SiGe HBTs with area of 1x20 μm^2 and 5x20 μm^2 were measured with the setup described above and C_T was extracted. A measured and simulated curve of V_c versus frequency for a device with an area of 5x20 μm^2 can be seen in Fig. 3. Due to parasitic reactances between the base and collector pads, the attenuation at higher frequencies was affected, but this has been accurately modeled and accounted for.
A measurement in the time domain of the 5x20 μm^2 device was performed using a setup like in Fig. 2. The device was fed a constant base current. A large-signal voltage step increased the power dissipation of the device and the large signal output, v_C, was then measured. From this resulting signal, a temperature dependent collector current was calculated. Using simulations with the extracted thermal capacitance, we find excellent agreement with the experiment in the temporal response.

Conclusion

A method to find the thermal time constant utilising small signal measurements in the frequency domain has been presented. Using an electrothermal model of an HBT, the method has been verified.

Acknowledgement

The authors wish to thank U. Erben and J. Schneider, University of Ulm, Germany, for helpful discussions.

References

[1] G.L. Skibinski, W.A. Sethares, "Thermal parameter estimation using recursive identifictaion," Conference record of the 1990 IEEE industry applications Society meeting, 1990, vol. 2, pp. 1581-1588.

[2] J. Zarebski, K. Gorecki, "A metod of the BJT transient thermal impedance measurement with double junction calibration," Eleventh annual IEEE semiconductor thermal measurement and management symposium, 1995, pp. 80-82.

[3] Z. Jakopovic, Z. Bencic, R. Zunac, "A correction of measured power MOSFETś normalized temperature response because of a case temperature rise," Fifth European conference on Power Electronics and applications, Brighton, England, 1993, vol. 2, pp. 143-148.

[4] S. Bruce, A. Rydberg, H. Schumacher, U. Erben, J-F. Luy, M. Karlsteen, M. Willander, "Development, implementation and verification of a physics-based Si/SiGe HBT model for millimeter-wave non-linear circuit simulations," 26th European Microwave Conference, Prague, Czech Republic, 1996, vol. 2, pp. 903-905.

[5] D.E. Dawson, A. K. Gupta, M. L. Salib, "CW measurement of HBT thermal resistance," IEEE Trans. Electron Devices, 1992, vol. 39, no. 10, pp. 2235-2239.

Paper IV

"Design and realization of a millimeter-wave Si/SiGe HBT frequency multiplier"

S. Bruce, A. Rydberg, M. Kim, F. Beiβwanger, J. F. Luy, H. Schumacher, U. Erben, M. Willander and M. Karlsteen

IEEE Trans. Microwave Theory Tech., vol. 46, no. 5, pp. 695 – 700, May 1998.

Design and Realization of a Millimeter-Wave Si/SiGe HBT Frequency Multiplier

Staffan P. O. Bruce, *Student Member, IEEE*, Anders Rydberg, *Member, IEEE*, Moonil Kim, *Member, IEEE*, Frank J. Beißwanger, J-F. Luy, *Senior Member, IEEE*, Hermann Schumacher, *Member, IEEE*, Uwe Erben, *Associate Member, IEEE*, Magnus Willander, *Member, IEEE* and Magnus Karlsteen

Abstract— **In this paper, the design of an active millimeterwave frequency doubler using an Si/SiGe heterojunction bipolar transistor (HBT) as the active device is studied. Simulations are made using a developed physics-based large-signal model for Si/SiGe HBT's, which includes thermal dependence. Despite the high output operating frequency of the fabricated doubler being close to f_{max}67 GHz for the Si/SiGe HBT, the conversion efficiency in a not completely optimized circuit is found to be better than -12 dB. The 3-dB bandwidth for the doubler is about 7.4%. These results are found to be comparable to a heterojunction field-effect transistor (HFET) doubler operating equally close to its f_{max}. Simulated results of the doubler performance with varied terminating impedances for the HBT are presented as design aids.**

I. Introduction

THE objective for investigating silicon-based (monolithic) microwave integrated circuit [(M)MIC] technology is the inherent possibility to realize millimeter-wave single-chip systems having advanced signal processing capabilities. Silicon-based active devices such as Si/SiGe heterojunction bipolar transistors (HBT's) have shown great potential of performance where devices with a maximum frequency of oscillation (f_{max}) of 70 GHz have been implemented in circuits and f_{max} of 160 GHz has been reached recently in common emitter configuration for single devices [1], [2]. Moreover, high-resistivity silicon which is the substrate material for millimeter-wave SiGe-based circuits, has been shown to give dielectric losses within the same order as semi-insulating GaAs at millimeter-wave frequencies [3].

In order to evaluate the feasibility of the SiGe technology for applications at millimeter-wave frequencies, demonstrators are being designed. A first demonstrator chosen for evaluation of the silicon-based (M)MIC-technology is a 55 GHz frequency multiplier using an HBT as the active device, having an f_{max} of 67 GHz. The frequency multiplier provides the opportunity to evaluate not only the application, but also non-linear models developed for the millimeter-wave SiGe HBT's. The majority of designs of active millimeter multipliers are based on FET devices as the non-linear component [4]-[5]. A frequency multiplier for lower microwave frequencies using an AlInAs/GaInAs/InP HBT was recently presented showing promising results [6]. As far as the authors know, no frequency multiplier for millimeter wave has been presented using an SiGe HBT as the active device.

Manuscript received November 5, 1996; revised September 6, 1997. This work was supported by the Swedish Board for Industrial and Technological Development (NUTEK) and by the ISS90 Foundation. The work of F. Beißwanger was supported under the state Baden-Württemberg program for the promotion of young-generation scientists

S. P. O. Bruce and A. Rydberg are with the Signals and Systems Group, Uppsala University, SE-751 20 Uppsala, Sweden.

M. Kim is with the Jet Propulsion Laboratory, Pasadena CA 91109 USA.

F. J. Beißwanger is with TEMIC Semiconductor GmbH, 74025 Heilbronn, Germany.

J-F. Luy is with Daimler-Benz Research, Microwave Techniques, D-89081 Ulm, Germany

H. Schumacher and U. Erben are with the Department of Electron Devices and Circuits, University of Ulm, D-89069 Ulm, Germany.

M. Willander is with Departemnt of Physics, Göteborg University and Charlmers University of Technology, Gothenburg S-41296, Sweden.

M. Karlsteen is with Chalmers University of Technology, Gothenburg S-41296, Sweden

Publisher Item Identifier S 0018-9480(98)03382-1.

II. HBT model

A large-signal model whose parameters can be directly related to the physical transistor has been developed for nonlinear applications. A modified Ebers-Moll model having transit time delay added to the current generator has been shown to sufficiently model HBT transistors at microwave frequencies [7]. The model has the benefit of taking into account the physical properties of the transistor and of having only a moderate number of parameters. Also of importance is that the variation of the technological parameters such as layer structure and geometries of the device can be accounted for.

The implementation of the model has been done in a SPICE-like simulator using a Microwave Design System (MDS) from Hewlett-Packard. A special feature in MDS called the symbolically defined device (SDD) has been used for modeling the intrinsic part of the transistor, schematically shown as the shaded part in Fig. 1(a).

For simplicity and computational speed, the model has been divided into three levels, each describing one part of the actual transistor where the lowest level mainly accounts for pad and contacting parasitics, using only linear elements. The middle level describes extrinsic parasitic resistances and reactances, some of which are bias dependent.

The highest level models the intrinsic part of the transistor (see Fig. 1(a), shaded part), where the aim has been to use elements that give a discrete analogy to the electrical processes occurring. For this reason, separate diodes are used in each junction to model the ideal electron and hole injection currents (I_{eF}, I_{eR}) and (I_{hF}, I_{hR}), respectively, where the indexes e, h, F and R denote electrons, holes, forward and reverse currents, respectively [see Fig. 1(a)]. As a result, αF and αR for the current generators in Fig. 1(a) do not need to account for electron injection efficiency which makes electrical modeling of thermal

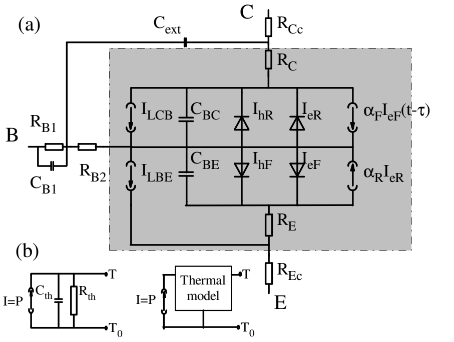

Fig. 1. Large signal HBT model: (a) electrical model, (b) examples of thermal equivalents for the circuit.

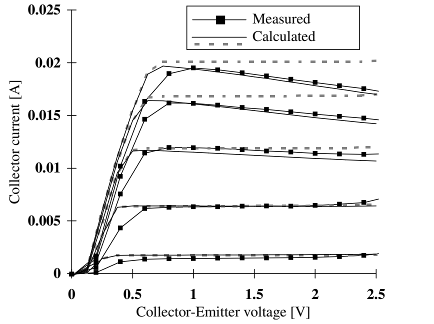

Fig. 2. Measured and calculated I-V characteristics for a 1x20 $\mu\mathrm{m}^2$ device varying I_B from 50 to 250 mA. Dotted line shows calculation without a thermal model, straight line shows calculation with thermal model.

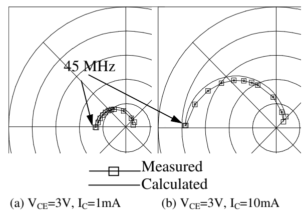

Fig. 3. Measured and calculated forward transmission (S_{21}) from 45 MHz to 50 GHz. DC-bias is 3V, 1mA (a) and 3V, 10mA (b). Full scale of the plots are 10. Pointed out in the graph is the starting frequency.

effects less complex. Since the electron and hole injection exhibit different thermal dependence due to different bandgaps in the different layers, a separate treatment of these currents make any function describing their interdependence in a unified diode superfluous. The current generators I_{LCB} and I_{LBE} have been added to empirically model high injection effects and the surface currents occurring on a mesa device structure. The capacitances C_{BE} and C_{BC} have been calculated using the SPICE model for junction depletion capacitances taking into account charge compensation in the collector space charge region which occurs at high collector currents for the base-collector capacitance C_{BC} [8].

Thermal modeling has been accomplished by creating an interface via the SDD, making it possible to use different complexities in the thermal model; from a lumped thermal resistance to nonlinear models derived from FEM-simulations, see Fig. 1(b). In this application, a lumped structure like the one in Fig. 1(b) is sufficient for finding the correct bias point.

The analytical expressions which the model parameters are based on are useful for a first estimation of transistor behavior. Starting values for the parameters are calculated from given device geometries, layer structure and known semiconductor properties. However, due to the complexity in the physical relations governing the semiconductor, and to uncertainties in the fabrication process, some of these parameters that are used in the calculations, inherently contain errors. Extraction and fitting of some model parameters to measured data is, therefore, necessary.

The measurements, performed at a known ambient temperature, result in Gummel, I-V plots and S-parameter curves at different bias. It is desirable to measure the S-parameters at low and high collector current and at least one intermediate value to get information of transistor behavior at the most important bias levels.

The fitting of parameters is done in a two-step process. Initially, only the technological parameters are allowed to vary within limits known from the fabrication process. Following this first step, elements in the equivalent circuit that do not directly relate to the intrinsic transistor are varied to further improve the accuracy of the model.

Parameters relating to nonidealities in the transistor-like leakage currents occurring on the surfaces of the collector and emitter and the base current at high injection have been extracted to achieve good agreement with measured dc characteristics. Additionally, certain resistors and time delays of the current generators are adjusted to best fit the measured S-parameters.

In order to verify the model, the electrical characteristics were calculated for a 1 μm × 20 μm emitter-area HBT with device geometry and layer structure similar to the one described in [9].

With some necessary adjustment of technological parameters due to inherent variations in the fabrication process, the resulting I-V characteristics and S-parameters have been calculated and compared to measurements (see Figs. 2 and 3). As can be seen, the simulated results agree with both the dc and RF measurements. The slightly sharper kink for simulated I-V characteristics in Fig. 2 at low V_{CE} and high I_C compared to the measured data is likely caused by a quasi-saturation creating a base pushout effect occurring when the base-collector junction is forward biased [10]. The typical decrease in β at high I_C with increasing V_{CE} is caused by the self-heating effect [8]. For comparison, the I-V characteristics have also been calculated without a thermal model (R_{th} in Fig. 1(b) is set to 0) (see Fig. 2).

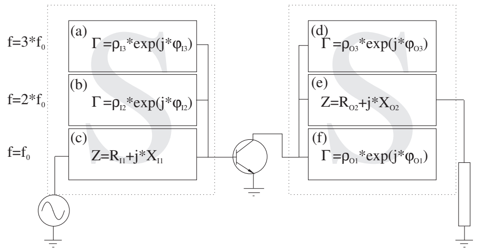

Fig. 4. A schematic presentation of the MDS model for the ideal doubler, used for optimization of matching circuit. Each block denotes one S-parameter block (shown with a shaded 'S').

The S-parameters are verified for a variation in collector current of one order of magnitude, thus making large-signal modeling plausible.

TABLE I
NOMINAL VALUES FOR OPTIMIZATION PARAMETERS IN DOUBLER STRUCTURE (SEE FIG. 4).

parameter	value	parameter	value
R_{I1}	19.7	ρ_{O1}	0.964
X_{I1}	42.7	φ_{O1}	90.0
ρ_{I2}	0.830	R_{O2}	57.8
φ_{I2}	221	X_{O2}	217

III. MULTIPLIER SIMULATION AND DISCUSSION

The simulation model for the doubler (see Fig. 4), developed in MDS, consists of separated ideal loads for the different frequencies of interest, i.e., fundamental, second and third harmonic respectively. The loads have been realized either as impedances or as reflection coefficients. The impedance coefficients have been used on the input for the fundamental frequency and on the output for the second harmonic [see Fig. 4(c) and (e)]. The latter have been used when a reactive low-loss termination is desirable [see Fig. 4(a), (b), (d) and (f)].

The process of designing the passive circuitry around the transistor has consisted of two conceptual steps which have been iterated to find an as optimal design as possible. In the first step, ideal impedances/reflection coefficients (described above) have been used. They have been optimized using assumptions that the circuit should as efficiently as possible match the transistor to 50 Ω on the input at the fundamental frequency and on the output at the second harmonic. Further, the input should block the second harmonic and the output should block the fundamental frequency.

In the second step, the calculated optimum impedances/S-parameters for the input and output circuits have been used for deriving a matching circuit using 50 Ω transmission lines shunted by shorted and open stubs. Since the resulting circuit does not have exactly the same characteristics as the ones found in the first step, it is necessary to recalculate the ideal input match-

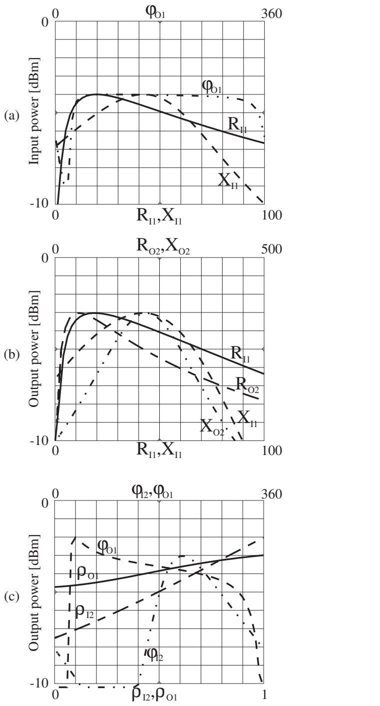

Fig. 5. Impact on input and output power from variation of matching parameters. One parameter was varied at a time. During optimization, source power was set to -4 dBm. (a) input power as a function of R_{I1}, X_{I1} and φ_{O1} (see Fig. 4). (b) output power as a function of R_{I1}, X_{I1} , R_{O2} and X_{O2} (see Fig. 4). (c) output power as a function of ρ_{O1}, ρ_{O2}, φ_{O1} and φ_{I2} (see Fig. 4).

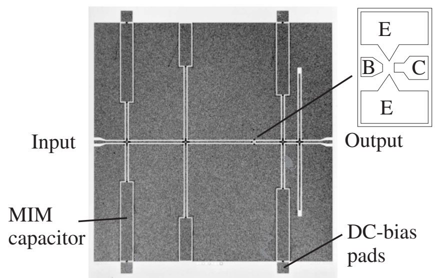

Fig. 6. The fabricated doubler circuit. A schematic of the transistor is shown on the right.

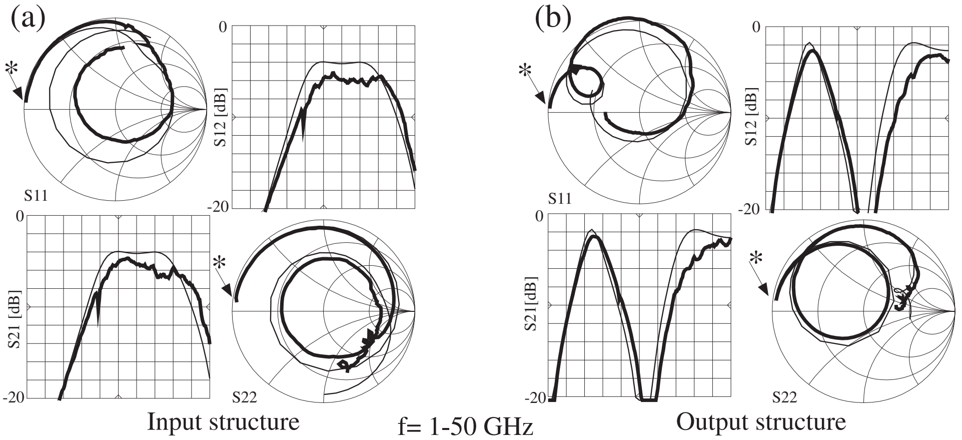

Fig. 7. Measured and calculated S-parameters for input and output matching circuit of the doubler circuit. Thin lines denote calculated data and thick lines denote measured data. The arrows in the Smith charts point out starting frequency. (a) input structure, port 2 connecting to transistor. (b) output structure, port 1 connecting to transistor.

ing circuit of the multiplier, setting the impedances on the output to the ones found in the second step. Further iterations, e.g., optimizing the output with given impedances on the input, did not improve the overall performance.

In the simulations, the impact from the terminations on the performance of the doubler has been studied by varying each of these around their nominal value in the optimized structure, keeping other parameters fixed at their optimal values (see Table I).

In doing so, it can be noticed that they either affect input matching or output power, but only some parameters affect both. This has been a great advantage when performing optimizations since fewer parameters have needed to vary for each goal function. As can be seen in Fig. 5(a), the input absorbed power is affected only by the input source impedance (see Fig. 4), and by the phase (φ_{O1}) of the reflection on the output, at the fundamental frequency. If the phase (φ_{O1}) can be kept away from the region where it strongly degrades input matching, it can be allowed to vary rather freely, having only moderate impact on the output power [see Fig. 5(c)]. Input matching is sensitive to the input impedance on the fundamental frequency and extra care needs to be taken not to have too low a resistive part since this clearly deteriorates performance.

The variation in input match as a function of R_{I2}, R_{I3}, R_{O1} and R_{O3} (see Fig. 4) was found to be negligible, due to small coupling between the harmonics and the fundamental frequency.

The output power [see Fig. 5(b) and (c)] also exhibits a clear dependence on the terminating impedances. Both the output match of the second harmonic and the input matching of the fundamental frequency obviously has a strong impact. The input matching has a similar dependence on the output power as on the absorbed input power [see Fig. 5(a) and (b)].

It can be seen that output power is very sensitive to variations in reflection coefficient at the second harmonic [see Fig. 5(c)] on the input – both regarding magnitude and phase. It can also be seen that the reflection coefficient at the fundamental frequency on the output affects the output power. Similar dependency of the reflection coefficients at the input and output has been found for FETs [11]. Finally, the simulations show that the impact from the third harmonic is negligible both on input and output power, and thus, they need not be considered during optimization.

In the design currently employed (see Fig. 6), the input uses two matching stubs (shorts) and the output structure consists of a matching stub (short) for the second harmonic frequency and a filter (open) to block the fundamental frequency. The matching circuit on the input and output also presents the HBT with the optimum terminating impedances for the fundamental and second harmonic frequency, respectively. The short circuit is accomplished with MIM- capacitors, thus making it possible to feed dc bias for the transistor on the center conductor of the coplanar waveguide.

To ensure a good understanding on how to realize the passive structures (shorts, opens, crosses and MIM capacitors), test circuits have been designed and fabricated using (EM) field simulators from Hewlett Packard [1]. Results from measurements on the passive structures conform well with simulated data up to at least 40 GHz (current limit of the measurement equipment used) (see Fig. 7).

IV. Measurements

The measurement setup for the evaluation of the fabricated doubler comprised of a HP8510C vector network analyzer for S-parameter measurements. A synthesized sweeper together with

[1] High-Frequency Structure Simulator (HFSS) and Momentum from Hewlett-Packard Corporation, Santa Rosa System Division, Santa Rosa, CA.

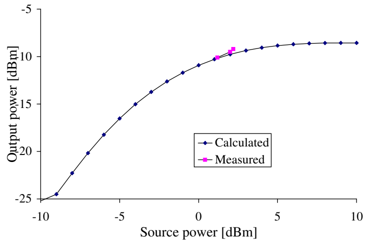

Fig. 8. Measured and calculated output power at 54.5 GHz versus source power at fundamental frequency for the doubler circuit.

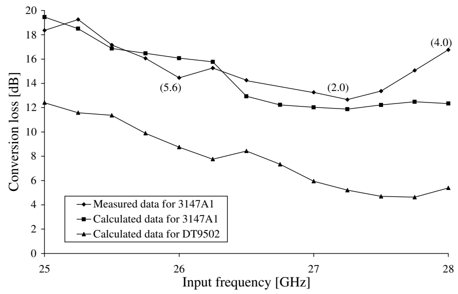

Fig. 9. Conversion loss versus frequency for the doubler circuit. Numbers within parenthesis depict source power at the input.

a power amplifier, was used for the power measurements. The circuit was contacted on input and output side using coplanar probes. The output power was measured using a waveguide V-band power sensor in order to further suppress the fundamental frequency being below the cutoff frequency of the waveguide. Measurements with the power amplifier setup using a through line instead of the doubler showed no detectable output signal at the harmonic frequency, thus showing that power delivered at the second harmonic only originated from the doubler itself.

The measured frequency doubler showed a conversion efficiency of better than -12 dB at an input power of 1.2 dBm and a dc bias of 4 V and 3 mA (see Fig. 8). It is to be observed that the efficiency calculated is defined as measured output power versus source power, thus the efficiency is better than the showed, taking into account mismatch on the input and output of the doubler. These results are found to be comparable to a heterojunction field-effect transistor (HFET) doubler operating equally close to its $f_{\max}$ [4]. The 3-dB power bandwidth for the multiplier was measured to be about 7.4% (see Fig. 9). The multiplier was originally designed for a Si/SiGe HBT (here called DT9502) having a different doping profile, thus having somewhat different S-parameters compared to the used device (here called 3147A1), which was available at the time of implementation. The difference in S-parameters between the devices implied that the used device (3147A1) is not optimally matched for working in this frequency multiplier. The effect of this difference in transistor behavior can be seen in Fig. 9, where the doubler structure has been simulated using both the DT9502 and 3147A1 as the active device. Fig. 9 shows the calculated conversion efficiency for the doubler using the derived HBT model and the calculated impedances for the input and output embedding circuits. The good agreement between theory and experiments makes it possible to predict the conversion behavior for different HBT devices and improving the design of the doubler.

V. Conclusions

A frequency doubler for 55 GHz with a conversion efficiency of better than -12 dB, operating at an output frequency near $f_{\max}$ for the device, has been designed and realized.

We have also presented a physics-based large-signal Si/SiGe HBT model, which uses data given from the fabrication process for finding the model parameters. By fitting of a few parameters, it is possible to accurately model the large-signal behavior up to millimeter-wave frequencies, which has been shown with the simulated and designed doubler circuit.

Acknowledgements

The authors wish to thank U. Spitzberg and M. Birk, University of Ulm, Ulm, Germany, for help with measurements, F. Schäffler, University of Linz, Linz, Austria and J. Schneider, University of Ulm, Ulm, Germany, for useful discussions. The authors also wish to thank K. M. Strohm for continuous technological support, H. Kibbel for layer growth, A. Schüppen and A. Gruhle for essential comments regarding the HBT process, and D. Eisbrenner for technical support, all affiliated with the Daimler-Benz Research Center in Ulm, Ulm, Germany. The Hewlett Packard Company, Santa Rosa, CA, is acknowledged for donating the CAD-systems used in the simulations.

References

[1] F. Beißwanger, U. Güttich, and C. Rheinfelder, "Microstrip and coplanar SiGe-MMIC oscillators," in *Proceedings of the 26th European Microwave Conference*, Prague, 1996, pp. 588–590.

[2] A. Schüppen, U. Erben, A. Gruhle, H. Kibbel, H. Schumacher, and U. König, "Enhanced SiGe heterojunction bipolar transistors with 160 GHz fmax," in *IEEE International Electron Devices Meeting (IEDM '95) Technical Digest*, 1995, pp. 30.4.1–30.4.4.

[3] J-F. Luy, K. M. Strohm, H-E. Sasse, A. Schüppen, J. Buechler, M. Wollitzer, A. Gruhle, F. Schäffler, U. Guettich, and A. Klaaßen, "Si/SiGe MMIC's," *IEEE Transactions on Microwave Theory and Techniques*, vol. 43, pp. 705–714, April 1995.

[4] H. Zirath, I. Angelov, N. Rorsman, C. Karlsson, and E. Kollberg, "A balanced W-band HFET doubler," in *Proceedings of the 23rd European Microwave Conference*, Madrid, 1993, pp. 837–839.

[5] M. Funabashi, T. Inoue, K. Ohata, K. Maruhashi, K. Hosoya, M. Kuzuhara, K. Kanekawa, and Y. Kobayashi, "A 60GHz MMIC stabilized frequency source composed of a 30GHz DRO and a doubler," in *IEEE MTT-S International Microwave Symposium Digest*, 1995, pp. 71–74.

[6] H. J. De Los Santos, D. D. Nardi, K. L. Hargrove, M. Hafizi, and W. E. Stanchina, "High-efficiency InP-based DHBT active frequency multipliers for wireless communications," *IEEE Transactions on Microwave Theory and Techniques*, vol. 44, pp. 1165–1167, July 1996.

[7] D. A. Teeter, J. R. East, R. K. Mains, and G. I. Haddad, "Large-signal numerical and analytical HBT models," *IEEE Transactions on Electron Devices*, vol. 40, no. 5, pp. 837–845, May 1993.

[8] Q. M. Zhang, J. Hu, J. Sitch, R. K. Surridge, and J. M. Xu, "A new large signal HBT model," in *IEEE MTT-S International Microwave Symposium Digest*, San Diego, 1994, pp. 1253–1256.

[9] A. Gruhle, H. Kibbel, U. König, U. Erben, and E. Kasper, "MBE-grown Si/SiGe HBTs with high ß, ft, and fmax," *IEEE Electron Device Letters*, vol. 13, pp. 206–208, 1992.
[10] G. M. Kull, L. W. Nagel, S-W. Lee, P. LLoyd, E. J. Prendergast, and H. Dirks, "A unified circuit model for bipolar transistors including quasi-saturation effects," *IEEE Transactions on Electron Devices*, vol. ED-32, pp. 1103–1113, June 1985.
[11] C. Rauscher, "High-frequency doubler operation of GaAs field-effect transistors," *IEEE Transactions on Microwave Theory and Techniques*, vol. MTT-31, pp. 462–473, June 1983.

Paper V

"Measurement of low-frequency base and collector current noise and coherence in SiGe heterojunction bipolar transistors using transimpedance amplifiers"

S. Bruce, L. K. J. Vandamme and A. Rydberg

IEEE Trans. Elec. Devices, vol. 46, pp. 993–1000, May 1999.

Measurement of Low-Frequency Base and Collector Current Noise and Coherence in SiGe Heterojunction Bipolar Transistors Using Transimpedance Amplifiers

Staffan P. O. Bruce, *Student Member, IEEE,* L. K. J. Vandamme, *Member, IEEE,* and Anders Rydberg, *Member, IEEE*

***Abstract*—Transimpedance amplifiers have been used for direct study of current noise in silicon germanium (SiGe) heterojunction bipolar transistors (HBT's) at different biasing conditions. This has facilitated a wider range of resistances in the measurement circuit around the transistor than is possible when using a voltage amplifier for the same kind of measurements. The ac current amplification factor h_{fe} and the sum of the base and emitter series resistances $(r_b + r_e)$ have been extracted from the noise. It has been established that the dominant noise source is situated in the base emitter junction at the emitter side and is not related to contact resistance noise. The simultaneous measurement of both the base-lead noise and the collector-lead noise and the calculation of the coherence between the signals has facilitated the pinpointing of the dominant noise source in the device and the extraction of $(r_b + r_e)$.**

***Index Terms*— HBT, low-frequency noise, silicon germanium (SiGe), transimpedance amplifiers.**

I. Introduction

The major source of phase noise in microwave oscillators is the transistor low-frequency noise which modulates the carrier [1]. Therefore low-frequency investigations on prototype microwave transistors are a first step in trying to optimize the phase noise of an oscillator. The general approach up to now for studying the $1/f$ noise in bipolar transistors is to use voltage amplifiers to measure the voltage fluctuations over a resistor which forms part of the measurement setup. By dividing the fluctuations in the voltage drop by the resistance value, a corresponding current noise is calculated. A first successful attempt has been carried out [2], [3] to use low-noise voltage amplifiers in Si bipolar transistors. Their configuration limits however the range of source and load resistances that can be used within the measurement. The present work aims at studying the current noise in base and collector current and their coherence in silicon germanium (SiGe) heterojunction bipolar transistors (HBT's) in a direct way, making use of ultra low-noise transimpedance amplifiers with or without internal biasing possibilities for measuring the current noise. These particular devices have been chosen for their pronounced noise in order to facilitate distinct measurements. Analysing the results shows where the dominant noise source is located. We will point out benefits and shortcomings with this technique.

Manuscript received October 7, 1998; revised December 17, 1998. The review of this paper was arranged by Editor W. Weber. This work was supported in part by The Swedish Strategic Foundation (SSF) through the microelectronics consortium “HF Bipolar Technology.”

S. Bruce and A. Rydberg are with Uppsala University, Uppsala, Sweden.

L. K. J. Vandamme is with the Eindhoven University of Technology, The Netherlands.

Publisher Item Identifier S 0018-9383(99)03514-5.

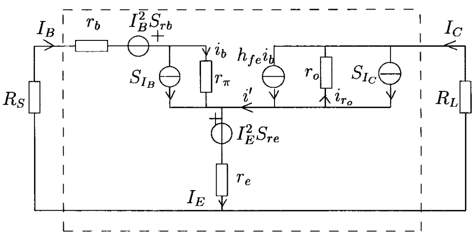

Fig. 1. Equivalent small signal circuit for an HBT in a common emitter measurement setup indicating the fundamental noise sources. The circuit inside the dotted rectangle corresponds to the transistor itself. I_B and I_E indicate steady state currents.

II. Theory

The noise sources of a bipolar transistor can schematically be presented as in Fig. 1 where the representation is made using resistance and current noise sources. S_{r_b}, S_{r_e}, S_{I_B}, and S_{I_C} are the resistance fluctuations of the base and emitter resistances and the current fluctuation in the base-emitter junction and in the collector, respectively. The steady state currents are indicated by I_B and I_E and cause a voltage fluctuation as a result of S_{r_b} and S_{r_e}; $h_{\rm fe}$ is the ac current amplification factor; r_π and r_o are the dynamic input and output resistances of the transistor; r_b and r_e are the base and emitter resistances within the transistor and R_S and R_L are the source and load resistances within the measurement setup.

These sources can be further decomposed into different types of noise. S_{I_B} and S_{I_C} consist of shot noise, generation-recombination (GR) noise and $1/f$ noise

$$S_{I_B} = 2qI_B + S_{I_B}^{1/f} + S_{I_B}^{GR} \tag{1}$$

$$S_{I_C} = 2qI_C + S_{I_C}^{1/f} + S_{I_C}^{GR}. \tag{2}$$

Similarly, in general the sources due to conductance fluctuations (S_{r_b} and S_{r_e}) can be composed of GR noise, random telegraph signal (RTS) noise and $1/f$ noise. The resistances r_b and r_e also contribute with Nyquist noise. The Nyquist noise can be seen as voltage sources in series with $I_B^2 S_{r_b}$ and $I_E^2 S_{r_e}$, but due to the heavy doping of both the base and the emitter, facilitated by the heterostructure, this noise is very low and has not been detected in measurements. They are thus not included in Fig. 1. Also the GR and RTS noise have not been observed and are therefore ignored in the discussion. From the equivalent circuit in Fig. 1 the theoretical expressions for the measured noise current spectra in the base ($S_{I_{BE}}$) and the collector-lead ($S_{I_{CE}}$) have been derived in the Appendix and are expressed as

$$S_{I_{BE}} = \frac{1}{Z^2}\left[I_B^2 S_{r_b} + r_\pi^2 S_{I_B} + I_E^2 S_{r_e} + r_e^2 S_{I_C}\right] \quad (3)$$

$$S_{I_{CE}} = \frac{h_{\text{fe}}^2}{Z^2}\left[I_B^2 S_{r_b} + Z_S'^2 S_{I_B} + {I_E}^2 S_{r_e} + \frac{(R_S + r_b + r_\pi + r_e)^2}{h_{\text{fe}}^2} S_{I_C}\right]. \quad (4)$$

The correlated spectrum between the two signals is expressed as

$$S_{I_{BE}I_{CE}} = \frac{h_{\text{fe}}}{Z^2}\left[I_B^2 S_{r_b} - r_\pi Z_S' S_{I_B} + I_E^2 S_{r_e} - \frac{(R_S + r_b + r_\pi + r_e) r_e}{h_{\text{fe}}} S_{I_C}\right] \quad (5)$$

where

$$Z = (R_S + r_b + r_\pi + (1 + h_{\text{fe}}) r_e) \quad (6)$$

$$Z_S' = (R_S + r_b + r_e) = Z - r_\pi - h_{\text{fe}} r_e \quad (7)$$

$$I_E = (1 + \beta) I_B.$$

Normally, in the active region, $(r_o/(R_L + r_o)) \approx 1$; and β is the dc part of the current amplification factor. The minus sign in (5) is related to the different directions of the currents that this source generates in the two measurement leads. For the coherence defined as (the full expression can be found in the Appendix)

$$\gamma^2 \stackrel{\text{def}}{=} \frac{S_{I_{BE}I_{CE}}^2}{S_{I_{BE}} \cdot S_{I_{CE}}} \quad (8)$$

holds $\gamma^2 = 1$ when a single noise source is dominant in both measurement leads, independent of R_S and R_L.

In practice, the correlated spectrum ($S_{I_{BE}I_{CE}}$) is calculated through a multiplication in the frequency domain between the complex Fourier transforms of the the two measured signals whose spectral power densities are $S_{I_{BE}}$ and $S_{I_{CE}}$. The coherence function is then calculated using its definition in (8).

III. Measurement Setup

Using a measurement setup like the one in Fig. 2(a), current noise can be directly measured for a variety of lead resistances of the base [R_S in Fig. 1 and Fig. 2(a)]. Also the lead resistance of the collector can be varied, in order to find information regarding the dynamic output resistance. In this investigation the external resistance in the collector lead has been held as low as possible which means that the nonnegligible internal resistance of the transimpedance amplifier in this lead has been dominating the resistance. This ensures that the whole noise current is measured. Due to the very low feedback from collector to base, the variation in impedance when changing range setting of the amplifier in the collector-lead does not affect the electrical behavior of the circuit and can thus be neglected.

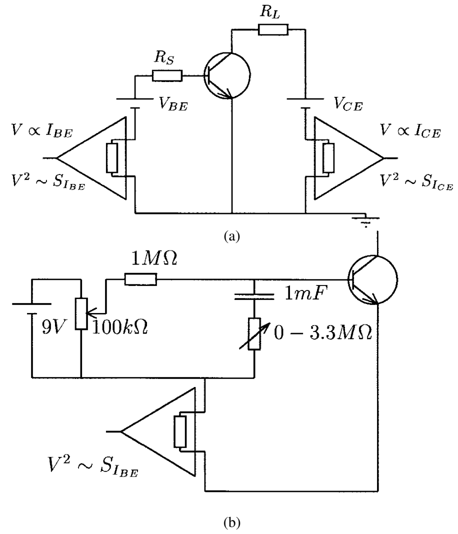

Fig. 2. Measurement setup. (a) The current passing through the transimpedance amplifiers are converted to an equivalent voltage which is measured using a double-channel low-frequency spectrum analyzer with the possibility to calculate the coherence between the two channels. (b) A close up of the biasing of the base current facilitating a precise control of the dc bias current and of the ac load impedance.

Assuming the noise sources as shown in Fig. 1, the measured noise in the base-lead ($S_{I_{BE}}$) and in the collector-lead ($S_{I_{CE}}$) can be used for extracting information regarding the different noise sources within the device. Some advantages and drawbacks of transimpedance amplifiers will be discussed.

In order to keep control of the measurements, two different types of transimpedance amplifiers have been used for converting the measured current to a corresponding voltage: Brookdeal 5002 and Stanford Research Systems SR570. The latter facilitates internal voltage bias with a high resolution which can be controlled by a computer. This showed very useful when performing sweeps of the base current. However, caution must be taken not to nonintentionally induce noise in the system by using this internal voltage source. The Brookdeal 5002 does not have an internal biasing and induces very little noise into the measurement setup. An external voltage source with variable ac impedance [see Fig. 2(b)] has been realized, mainly based on a battery, a high-quality potentiometer and a variable resistance in series with a large capacitance. If the measuring of dc part of the current can be omitted, the transimpedance amplifier can be inserted in direct series with the capacitance and the variable resistance which can enable a higher amplification factor as the amplifier does not need to sink the dc current. A higher amplification factor results however also in a higher internal impedance within the amplifier which must be accounted for.

Measuring the noise currents directly with transimpedance amplifiers enables us to use a large range in source resistances. The only limitation is that the impedance of the measured circuit should be larger than the input impedance of the current amplifier. This is easily obtained with transistors where the dynamic resistance always is much higher than the input impedance of the amplifier for all current levels. This enables simultaneous measurements of both the base and collector current noise and calculation of their coherence directly. The measurements would be very difficult to perform using voltage amplifiers at low values of the source resistances since the signal would be drowned in the Nyquist noise of the resistor itself and the background noise of the amplifier. As an example, a measurement of the shot noise level, calculated as $2qI$, using a 1 kΩ resistor and a voltage amplifier means the current I must be higher than 50 μA in order not to be drowned by the internal Nyquist noise of the resistor. This is a high current for small devices. Lower current noise levels would thus not be possible to detect without severely degrading the coherence calculation between the two measured signals due to uncorrelated noise contributions of the resistances R_L and R_S.

By changing the sensitivity of the transimpedance amplifier, its internal impedance changes which appears as a variation in source impedance for the device under test. Attention to this behavior is given during measurements of current sweeps since both $S_{I_{BE}}$ and $S_{I_{BC}}$ can be affected by variation in impedance.

High current sensitivity goes hand in hand with a higher input impedance and a lower bandwidth. In addition to a limited bandwidth, the transimpedance amplifier exhibits an inductive behavior at the input which can introduce a resonance with a (parasitic) capacitance at the input. For this work, either a frequency of 20, 25, or 170 Hz has been chosen when comparing results of different bias conditions; mainly in order to avoid disturbance from harmonics of the 50 Hz power line signal, background noise and bandwidth problems. The reason for choosing the higher frequency of 170 Hz is due to the series capacitance for the ac impedance in the base lead [see Fig. 2(b)].

The internal bias supply of the SR570 amplifier enables a very compact solution for the measurement setup which makes it less prone to picking up undesired signals. However, owing to the very high open loop gain of the amplifier in the internal transimpedance stage, any fluctuation in the reference voltage for the bias will appear as an almost ideal voltage noise source at, e.g., the base of the transistor. This will affect both $S_{I_{BE}}$ and $S_{I_{CE}}$ and in worst case induce an undesired full coherence between the two measured noise signals. The same undesired noise source can also be unevenly partitioned between the two channels, especially for low values of R_S, where $S_{I_{CE}}$ is affected, which can result in a low coherence. Here the results of coherence between $S_{I_{BE}}$ and $S_{I_{CE}}$ without measurement artifacts will be presented by the usage of the Brookdeal 5002 where the SR570 is found insufficient after comparing the results with a Brookdeal 5002.

IV. Results

Measured current noise spectra of a 20-μm^2 device for the base-lead and collector-lead is shown in Fig. 3. The curves indicate a spectra with $1/f^{0.8}$ dependence below 10 kHz which is in accordance with results for similar devices [4]. The level of the noise is too high for any white noise to be seen within the measured frequency range. Furthermore, the noise measurements at low currents are limited by the bandwidth of the amplifier which can be seen as a distinct roll-off above 10 kHz. A plot of coherence between the two noise spectra measured at any given base current shows a value very close to unity, see Fig. 3. This indicates that the measured noise originates from a common source, thus excluding any dominant source in the collector-lead and hence S_{I_B}, S_{r_b}, or S_{r_e} are the possible candidates.

In order to discriminate, we measure the current spectra at approximately constant values of base and collector current for a range of source resistances (R_S in Fig. 2). We deduce from (4) and (7) and our experimental results that S_{I_B} is the single dominant source for almost all values of R_S. A more thorough explanation will follow.

As can be seen in Fig. 4, $S_{I_{CE}}$ shows a square dependence on R_S for values of 300 $\Omega \leq R_S \leq r_\pi$ which indicates strongly that S_{I_B} can be the only source, as can be seen from the second term in (4). All other components in (4) are for these values of R_S either independent of, or only very weakly dependent on R_S. In this region of R_S, the coherence (γ) is very close to unity, thus indicating that the same source is totally dominant also in $S_{I_{BE}}$. This means however that S_{I_B} is dominant in $S_{I_{BE}}$ for all values of R_S since the interdependence between the different terms in $S_{I_{BE}}$ is independent of R_S, [see (3)].

For low values of R_S, the coherence goes down (see Fig. 4) which indicates that at least one additional source (here called S_X) becomes significant in $S_{I_{CE}}$. The origin of this source is difficult to distinguish as the measured noise levels at these values of R_S are very low and thus external noise may enter, but from (5) or (36), shown at the bottom of the page, it can be indicated that S_{I_C} is a candidate since γ^2 never drops to zero. To pinpoint the source, a more thorough investigation would however be necessary which is beyond the scope of this paper. Assuming that this source is independent of R_S and bearing in mind that $S_{I_{BE}}$ is completely dominated by S_{I_B}, S_X is calculated as

$$S_X = (1 - \gamma^2) S_{I_{CE}}. \tag{9}$$

The coherence does however not reach zero for the given range of R_S thus indicating that S_{I_B} still contributes to $S_{I_{CE}}$. This level is calculated (here called $S_{I_{CE_1}}$) as

$$S_{I_{CE_1}} = \gamma^2 S_{I_{CE}} \tag{10}$$

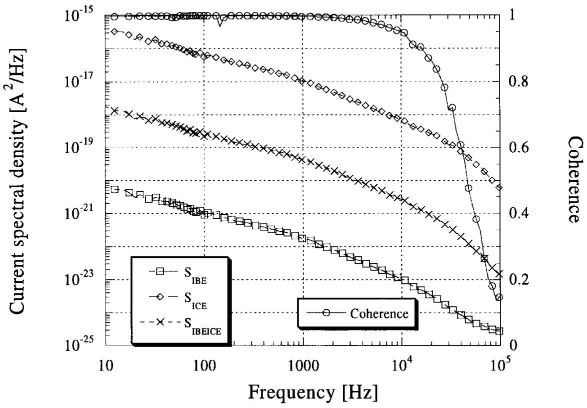

Fig. 3. Measured current noise spectrum through the base and collector-lead for a 20 μm^2 device. Coherence between the two signals is included. The source resistance is set to $R_S = 10$ kΩ and I_B was set to 1 μA. The roll-off at higher frequencies for the curves is due to the limited bandwidth of the transimpedance amplifiers.

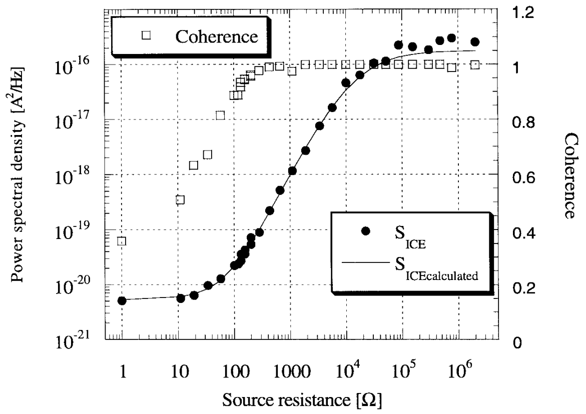

Fig. 4. Measured and calculated data of $S_{I_{CE}}$ versus R_S for a 24 μm^2 device at $V_{CE} = 1.5$ V, $I_B = 2$ μA and $f = 170$ Hz. Calculated data ($S_{I_{CE_{\text{calculated}}}}$) using (13). Coherence is also included.

and the value of $(R_S + r_b + r_e)$ can be extracted as a factor in front of S_{I_B}, see (3). Note that in this region, $R_S \ll r_\pi$.

For the extraction, a measurement (here called $S_{I_{CE_2}}$) of $S_{I_{CE}}$ is taken where S_{I_B} is dominant and $R_S \gg (r_b + r_e)$. The quotient between $S_{I_{CE_1}}$ and $S_{I_{CE_2}}$ will then be (neglecting insignificant terms)

$$\frac{S_{I_{CE_1}}}{S_{I_{CE_2}}} = \left(\frac{(R_{S_1} + r_b + r_e)(R_{S_2} + r_\pi)}{R_{S_2} r_\pi}\right)^2 \tag{11}$$

and $(r_b + r_e)$ is found as

$$(r_b + r_e) = \sqrt{\frac{S_{I_{CE_1}}}{S_{I_{CE_2}}}} \left(\frac{R_{S_2} r_\pi}{R_{S_2} + r_\pi}\right) - R_{S_1} \tag{12}$$

where R_{S_1} and R_{S_2} are the values of R_S for the measurements of $S_{I_{CE_1}}$ and $S_{I_{CE_2}}$, respectively. An average of the extracted values for $R_{S_1} = 1$, 11, 19, and 34 Ω (indicating values of $S_{I_{CE}}$ where the coherence clearly differs from unity) and $R_{S_2} = 3.4$ kΩ gives $S_X = 4.4 \cdot 10^{-21}$ A^2/Hz at $f = 170$ Hz and $(r_b + r_e) = 28\,\Omega$.

Under the assumption that only the sources S_{I_B} and S_X contribute to $S_{I_{CE}}$, a simplified expression is found as

$$S_{I_{CE_{\text{calculated}}}} = S_{I_{CE_0}} \left(\frac{Z'}{Z}\right)^2 + S_X. \tag{13}$$

Thus, only one additional parameter, here called $S_{I_{CE_0}}$, needs to be extracted to be able to calculate $S_{I_{CE}}$. From (4) it

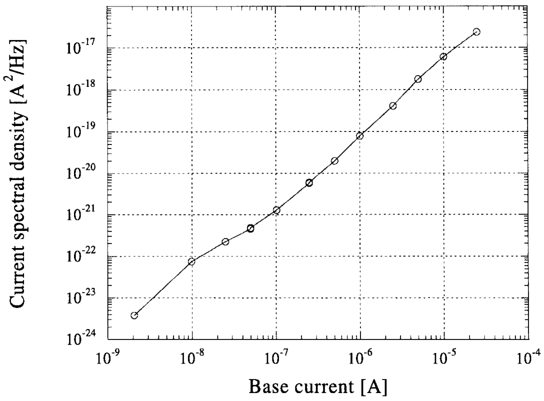

Fig. 5. Extracted values of S_{I_B} versus I_B on a 20 $\mu\mathrm{m}^2$ device. Measurements done at $f = 25$ Hz, $V_{CE} = 1.5$ V and $R_S = 100$ kΩ.

is found that this corresponds to $h_{\mathrm{fe}}{}^2 S_{I_B}$. However, in order to gain as much information as possible from the measured $S_{I_{CE}}$ and not include uncertainty from additional circuit parameters, a calculation of this term is omitted in favor of a direct extraction. In a region where $(r_b + r_e) \ll R_S < r_\pi/2, S_{I_B}$ is dominant, $S_{I_{CE_0}}$ is found as

$$S_{I_{CE_0}} = S_{I_{CE}} \left(\frac{R_S + r_\pi}{R_S + (r_b + r_e)} \right)^2. \tag{14}$$

For $500\ \Omega \leq R_S \leq 6\ \mathrm{k}\Omega$ and $f = 170$ Hz an average of $S_{I_{CE_0}}$ was found to be $1.8 \cdot 10^{-16}\ \mathrm{A}^2/\mathrm{Hz}$. This compares very well with the calculated value found using extracted h_{fe} and S_{I_B}.

The curve of $S_{I_{CE_{\mathrm{calculated}}}}$ has been included in Fig. 4 as a full line and compares very well with measured data (dots), thus showing that the assumptions are correct. From the shape of $S_{I_{CE}}$, it can be seen that there is a lower limit to which there is any point in setting the biasing impedance, R_S, and this is above the value of $(r_b + r_e)$. Furthermore, as biasing impedance increases, $S_{I_{CE}}$ rolls off, indicating that bias impedances chosen above the value of r_π does not further increase $S_{I_{CE}}$. An implication of this is that devices with a high β will have a high range of $S_{I_{CE}}$ depending on which biasing impedance is chosen since I_B here is small and thus r_π becomes large, giving a large span of values between $(r_b + r_e)$ and r_π.

Using (4) and (5), a value for h_{fe} is found as

$$h_{\mathrm{fe}} = \frac{S_{I_{CE}}}{S_{I_{BC}I_{CE}}} \frac{r_\pi}{R_S} \tag{15}$$

assuming $R_S \gg (1 + h_{\mathrm{fe}})r_e, S_{I_B}$ is the dominant noise source and $(r_o/(R_L + r_o)) \to 1$. Extracted values using (15) and data from the Gummel plot are compared in Table I.

A value of S_{I_B} is calculated as

$$S_{I_B} = S_{I_{BE}} * \frac{(R_S + r_\pi)^2}{r_\pi^2} \tag{16}$$

TABLE I
EXTRACTED VALUES OF h_{fe} FOR A 20 $\mu\mathrm{m}^2$ DEVICE AT DIFFERENT VALUES OF I_B USING (15). $f = 25$ Hz, R_S 100 kΩ AND $V_{CE} = 1.5$ V. THE COLUMN $\delta I_C/\delta I_B$ INDICATES EXTRACTED DATA FROM A GUMMEL PLOT

I_B		h_{fe}	$\frac{\delta I_C}{\delta I_B}$
20	nA	35	38
200	nA	48	58
1	μA	64	79
2.6	μA	110	108
10	μA	120	177

for values of $R_S \gg r_b + (1 + h_{\mathrm{fe}})r_e$. In particular, for $(r_b + (1 + h_{\mathrm{fe}})r_e) \ll R_S \ll r_\pi$ we have $S_{I_B} \approx S_{I_{BE}}$.

A dependence on base current of approximately $I_B^{1.7}$ has been measured throughout the available bias range, see Fig. 5. For currents below 250 nA, the frequency dependence if the noise is weaker and bandwidth limitations play a role. The reduced frequency dependence of S_{I_B} in conjunction with the current dependence indicate that the noise source is not of pure $1/f$-type and any real predictions on corner frequencies where the low-frequency noise disappears in the shot noise are difficult to make [5].

The current dependence of S_{I_B} gives space for interpretations of the origin of the noise. As shown earlier, the noise originates within the base-emitter junction which here means not in the base resistance and not in the emitter resistance. Assuming a true area dependent effect, the mobility fluctuation model or the number fluctuation model seem to be reasonable candidates. The Kleinpenning model considers mobility fluctuations and hence fluctuations in the diffusion coefficient for the minority carriers. A simplified relation, which indicates a linear dependence of S_{I_B} on current, is given as follows [6]:

$$S_{I_B} = \frac{2\alpha q I_B D_p}{f W_E^2} \tag{17}$$

where D_p is the hole diffusion coefficient in the emitter of an NPN transistor and W_E is the length of the undepleted part of the emitter. With $D_p = 5\ \mathrm{cm}^2/\mathrm{s},\ W_E = 1.2 * 10^{-5}$ cm and

$f = 25$ Hz, calculated α for $I_B = 250$ nA and $I_B = 25$ μA give values of $5 * 10^{-5}$ and $2 * 10^{-3}$, respectively, which is within reasonable limits [7]. Due to the variation in base current, the depletion region in the emitter vary and thus also the region where the fluctuation in mobility will be of greatest importance. The fact that α is nonuniform can speak for a position dependence on α in the W_E region just at the rim of the depletion region [8].

The number fluctuation model considers a fluctuation in the surface recombination velocity, s. With the relation for short diodes [9]

$$\frac{S_I}{I^2} = C \cdot S_s \tag{18}$$

where C is independent of current and S_s is the spectral density of the fluctuations in s with a $1/f$-type of spectrum. It can be seen that this model predicts a square-law dependence on current just like series resistance fluctuations. This model thus fits to the "near-square-law" dependence of S_{I_B} which has been observed.

V. Conclusion

We have used transimpedance amplifiers for direct study of current noise in a silicon germanium HBT at different biasing conditions. The possibility of measuring the device using a wider range of external resistances than is possible when using a voltage amplifier has facilitated extraction of the ac current amplification factor h_{fe} and the sum of the base and emitter series resistances $(r_b + r_e)$. The simultaneous measurement of both the base-lead noise and the collector-lead noise has enabled a calculation of the coherence between the signals. From the high coherence and the dependence of collector-lead noise on source resistance, it has been established that the dominant noise source is situated in the base emitter junction, in the W_E region at the emitter side and not in the contact resistances r_b and r_e. The use of the coherence function has been essential for the discrimination of the dominant noise source and for the extraction of $(r_b + r_e)$.

Appendix
Derivation of $S_{I_{CE}}, S_{I_{BE}}, S_{I_{BE}I_{CE}}$, and γ^2 and Estimation of the Impact of S_{I_C} on the Measurements

This Appendix gives a more thorough description of how the important expressions for $S_{I_{CE}}, S_{I_{BE}}, S_{I_{BE}I_{CE}}$, and γ^2 [(3)–(5) and (8)] are derived. The expressions will be derived in steps, concentrating on one source at a time and finally collecting the the different parts to the full expressions.

A. Derivation of $S_{I_{CE}}, S_{I_{BE}}$, and $S_{I_{BE}I_{CE}}$ with Respect to S_{I_C}

The emphasis is first put on finding the impact of a noise source in the collector lead on the noise in the base lead. From Fig. 1, we define the following currents when S_{I_C} is the only contributor:

$$\begin{cases} i' = i_{S_{I_C}} - i_{r_o} + h_{\text{fe}} i_b \\ i_b = -i' \dfrac{r_e}{R_S + r_b + r_\pi + r_e} \\ i_{r_o} = i' \dfrac{R_L + (R_S + r_b + r_\pi) \| r_e}{r_o}. \end{cases} \tag{19}$$

Elimination then gives (20) and (21), shown at the bottom of the page, where

$$(R_S + r_b + r_\pi) \| r_e \stackrel{\text{def}}{=} \frac{(R_S + r_b + r_\pi) * r_e}{(R_S + r_b + r_\pi) + r_e}. \tag{22}$$

For a common emitter configuration, $r_o, r_\pi \gg r_e$ and R_L can be chosen very small and it is thus possible to assume that $r_o, r_\pi \gg (r_e + R_L)$, thus

$$i_b = -\, i_{S_{I_C}} \frac{r_e}{Z} \tag{23}$$

$$i' = i_{S_{I_C}} \frac{R_S + r_b + r_\pi + r_e}{Z} \tag{24}$$

where

$$Z = (R_S + r_b + r_\pi + (1 + h_{\text{fe}}) r_e).$$

It can be seen in Fig. 1 that i' is the same as the current flowing through R_L. Straightforward circuit analysis thus gives

$$\begin{aligned} S_{I_{BE}} &= \frac{{r_e}^2 S_{I_C}}{Z^2} \\ S_{I_{CE}} &= \frac{h_{\text{fe}}^2}{Z^2} \frac{(R_S + r_b + r_\pi + r_e)^2}{h_{\text{fe}}^2} S_{I_C} \end{aligned}.$$

Again it has been assumed that $r_o \gg (r_e + R_L)$.

The correlated spectrum between the two signals is expressed as [in the text (5)]

$$S_{I_{BE} I_{CE}} = \frac{h_{\text{fe}}}{Z^2} \frac{(R_S + r_b + r_\pi + r_e) r_e}{h_{\text{fe}}} S_{I_C}.$$

Can the source in the collector lead (i.e., S_{I_C}) be dominant?

If this is the case, we should find for the quotient between the power spectral densities of the measured signals

$$\frac{S_{I_{CE}}}{S_{I_{BE}}} = \left(\frac{R_S + r_b + r_\pi + r_e}{r_e} \right)^2. \tag{25}$$

$$i_b = -\, i_{S_{I_C}} \left[\frac{r_e}{R_S + r_b + r_\pi + r_e} \right] \left\{ \frac{1}{1 + \dfrac{R_L + (R_S + r_b + r_\pi) \| r_e}{r_o} + h_{\text{fe}} \dfrac{r_e}{R_S + r_b + r_\pi + r_e}} \right\} \tag{20}$$

$$i' = i_{S_{I_C}} \frac{1}{1 + \dfrac{R_L + (R_S + r_b + r_\pi) \| r_e}{r_o} + h_{\text{fe}} \dfrac{r_e}{R_S + r_b + r_\pi + r_e}} \tag{21}$$

$$\gamma^2 = \frac{\left[I_B^2 S_{r_b} - r_\pi Z_S' S_{I_B} + I_E^2 S_{r_e} - \frac{(R_S + r_b + r_\pi + r_e) r_e}{h_{\rm fe}} S_{I_C}\right]^2}{[I_B^2 S_{r_b} + (r_\pi + h_{\rm fe} r_e)^2 S_{I_B} + I_E^2 S_{r_e} + r_e^2 S_{I_C}]\left[I_B^2 S_{r_b} + Z_S'^2 S_{I_B} + I_E^2 S_{r_e} + \frac{(R_S + r_b + r_\pi + r_e)^2}{h_{\rm fe}^2} S_{I_C}\right]}. \quad (36)$$

For a base current $I_B = 1\,\mu$A, $r_\pi \approx 25\,\text{k}\Omega$. Assuming $r_e < 10\,\Omega$ which is well above the value found from dc analysis and neglecting R_S in order to get a worst case value, this gives from (25)

$$\frac{S_{I_{CE}}}{S_{I_{BE}}} > 6 \cdot 10^6.$$

However, at $I_B = 1\,\mu$A (see Fig. 3) the ratio between $S_{I_{CE}}$ and $S_{I_{BE}}$ is less than $5 \cdot 10^4$ and S_{I_C} can thus not be the dominant noise source.

B. *Derivation of $S_{I_{CE}}, S_{I_{BE}}$, and $S_{I_{BE}I_{CE}}$ with Respect to S_{r_b}, S_{r_e} and S_{I_B}, Ignoring S_{I_C}*

Call current flowing through R_S from basenode to ground as $i_{\rm be}$. Assume that the value of r_o is high which means it does not shunt any significant current in comparison with $h_{\rm fe} i_b$.

To begin with, we study the different components in $S_{I_{BE}}$. Looking first at the impact of S_{r_b}, i.e., this being the only source. Call voltage caused by ${I_B}^2 S_{r_b}$ as $u_{S_{r_b}}$. Kirchoffs law gives

$$u_{S_{r_b}} - i_b r_\pi - (i_b + h_{\rm fe} i_b) r_e + i_{\rm be} R_S - i_b r_b = 0. \quad (26)$$

Notice that $i_{\rm be} = -i_b$. This gives immediately

$$S_{I_{BE}} = \frac{I_B^2 S_{r_b}}{Z^2}. \quad (27)$$

Second, looking at the impact of S_{r_e}, i.e., this being the only source. Call voltage caused by $I_E^2 S_{r_e}$ as $u_{S_{r_e}}$. Kirchoff's law gives

$$u_{S_{re}} - (i_b + h_{\rm fe} i_b) r_e + i_{\rm be} R_S - i_b r_b - i_b r_\pi = 0. \quad (28)$$

Notice that $i_{\rm be} = -i_b$. This gives immediately

$$S_{I_{BE}} = \frac{I_E^2 S_{r_e}}{Z^2}. \quad (29)$$

Third, looking at the impact of S_{I_B}, i.e., this being the only source. Call current caused by S_{I_B} as $i_{S_{I_B}}$. Notice that

$$-i_{\rm be} - i_{S_{I_B}} - i_b = 0. \quad (30)$$

Kirchoff's law gives

$$i_{\rm be} R_S + i_{\rm be} r_b - i_b r_\pi - (i_{S_{I_B}} + i_b + h_{\rm fe} i_b) r_e = 0. \quad (31)$$

Substitution of i_b using (30) gives

$$i_{\rm be}(r_b + R_S + r_\pi + (1 + h_{\rm fe}) r_e) + i_{S_{I_B}}(r_\pi + h_{\rm fe} r_e) = 0 \quad (32)$$

which yields

$$S_{I_{BE}} = S_{I_B} \frac{(r_\pi + h_{\rm fe} r_e)^2}{Z^2} \quad (33)$$

and in total for all sources

$$S_{I_{BE}} = \frac{1}{Z^2}\,[I_B^2 S_{r_b} + (r_\pi + h_{\rm fe} r_e)^2 S_{I_B} + I_E^2 S_{r_e} + {r_e}^2 S_{I_C}]. \quad (34)$$

Continuing with $S_{I_{CE}}$, using the already found expressions [(26) and (28)], the impact on $S_{I_{CE}}$ from S_{r_b} and S_{r_e} can be found by noticing that in these cases $-i_{\rm be} = i_b$ and the current through R_L is $i_b h_{\rm fe}$ The impact of S_{I_B} on $S_{I_{CE}}$ can be found by using (30) and (32)

$$i_b = -i_{S_{I_B}}\left[\frac{R_S + r_b + r_e}{Z}\right]. \quad (35)$$

Thus, $S_{I_{CE}}$ will be

$$S_{I_{CE}} = \frac{h_{\rm fe}^2}{Z^2}\left[I_B^2 S_{r_b} + Z_S'^2 S_{I_B} + I_E^2 S_{r_e} + \frac{(R_S + r_b + r_\pi + r_e)^2}{h_{\rm fe}^2} S_{I_C}\right]$$

where

$$Z_S' = (R_S + r_b + r_e)$$

and $S_{I_{BE}I_{CE}}$ can be found as (noticing the direction of the different current components)

$$S_{I_{BE}I_{CE}} = \frac{h_{\rm fe}}{Z^2}\left[I_B^2 S_{r_b} - r_\pi Z_S' S_{I_B} + I_E^2 S_{r_e} - \frac{(R_S + r_b + r_\pi + r_e) r_e}{h_{\rm fe}} S_{I_C}\right].$$

C. *The Full Expression of γ^2*

Given the expressions for $S_{I_{BE}}, S_{I_{CE}}$, and $S_{I_{BE}I_{CE}}$, the expression for γ^2 can be calculated from its definition (8) and is found to be (36), shown at the top of the page.

ACKNOWLEDGMENT

The authors wish to thank an anonymous reviewer for comments improving the final manuscript. The authors are thankful to J. Briaire, Eindhoven University of Technology, The Netherlands, for providing a LabView program controlling the double-channel Advantest R9211E FFT spectrum analyzer. The work was done at Eindhoven University of Technology, The Netherlands.

REFERENCES

[1] O. Llopis, J. Verdier, M. Regis, R. Plana, M. Gayral, and J. Graffeuil, "Correlation between microwave transistors low-frequency noise, amplifiers residual phase noise and oscillators phase noise," in *Microwave Physics and Technique, Proceedings of the NATO Advanced Research Workshop*. Dordrecht, Netherlands: Kluwer, 1997, pp. 19–33.

[2] S. Jarrix, C. Delseny, F. Pascal, and G. Lecoy, "Noise correlation measurements in bipolar transistors. I. Theoretical expressions and extracted current spectral densities," *J. Appl. Phys.*, vol. 81, pp. 2651–2657, Mar. 1997.

[3] C. Delseny, F. Pascal, S. Jarrix, and G. Lecoy, "Noise correlation measurements in bipolar transistors. II. Correlation between base and collector currents," *J. Appl. Phys.*, vol. 81, pp. 2658–2665, Mar. 1997.

[4] L. Vempati, J. D. Cressler, J. A. Babcock, R. C. JAeger, and D. L. Harame, "Low-frequency noise in UHV/CVD epitaxial Si and SiGe bipolar transistors," *IEEE J. Solid-State Circuits*, vol. 31, pp. 1458–1467, Oct. 1996.

[5] A. Gruhle and C. Mähner, "Low $1/f$ noise SiGe HBT's with application to low phase noise microwave oscillators," *Electron. Lett.*, vol. 33, pp. 2050–2052, Nov. 1997.

[6] T. G. M. Kleinpenning, "Location of low-frequency noise in submicron bipolar transistors," *IEEE Trans. Electron Devices*, vol. 39, pp. 1501–1506, 1992.

[7] L. K. J. Vandamme, "Is the $1/f$ noise parameter α a constant?," in *Proc. 7th Int. Noise Conf., Noise in Physical Systems and* $1/f$ *Noise*, 1983, pp. 183–192.

[8] L. K. J. Vandamme, E. P. Vandamme, and J. J. Dobbelsteen, "Impact of silicon substrate, iron contamination and perimiter on saturation current and noise in n^+p diodes," *Solid State Electron.*, vol. 41, pp. 901–908, 1997.

[9] T. G. M. Kleinpenning, "$1/f$ noise in p-n junction diodes," *J. Vac. Sci. Technol. A*, vol. 3, pp. 178–182, Jan./Feb. 1985.

Staffan P. O. Bruce (S'94) was born in Göteborg, Sweden, in 1968. He received the M.Sc. degree in applied physics and electrical engineering from Linköping University, Sweden, in 1994. He is currently pursuing the Ph.D. degree at Uppsala University, Uppsala, Sweden.

His main interests concern modeling of high-frequency Si/SiGe HBT's, high-frequency applications, and $1/f$-noise in semiconductors.

L. K. J. Vandamme (M'99) was born in Panne, Belgium, in 1943. He received the B.S. degree from H. T. I. Oostende, Belgium, in 1965, the M.S. degree in electrical engineering (cum laude) from the Delft University of Technology, The Netherlands, in 1971, and the doctorate degree from Eindhoven University of Technology, The Netherlands, in 1976.

Currently, he is with the Eindhoven University of Technology, the Netherlands. He has done research on $1/f$ noise in electrical contacts, and thin- and thick-film resistors and optoelectronic devices. His current areas of research interest are $1/f$ noise in submicron MOSFET's, bipolar transistors and conductive adhesives. He has authored or coauthored more than 120 publications. During 1981–1982, 1987, 1992, and 1998, he was a Visiting Professor at the University of Science and Technology, Montpellier, France.

Anders Rydberg (M'89) was born in Lund, Sweden, in 1952. He received the M.Sc. degree from Lund Institute of Technology, Lund, in 1976, and the degree of Licentiate of Engineering and the Ph.D. degree from Chalmers University of Technology, Sweden, in 1986 and 1988, respectively.

He worked between 1977 and 1983 with the development and research at the National Defense Research Establishment, ELLEMTEL Development Company, and the Onsala Space Observatory. From 1990 to 1991, he was a Senior Research Engineer at Farran Technology Ltd., Ireland. In 1991, he was appointed Docent (Associated Professor) in Applied Electron Physics at Chalmers University of Technology. In 1992, he became Associated Professor at the Signal and Systems Group at Uppsala University School of Technology. Since 1996, he has also Associated Professor and Research Leader part-time at the University College Gävle-Sandviken. His main interests are micro- and millimeter-wave solid state components and circuits for radio communication. He has authored or coauthored more than 70 papers in the above research area. He is also a co-owner of one patent on applications of single-barrier-varactor diodes.

Dr. Rydberg is a member of the editorial board for IEEE TRANSACTIONS ON MICROWAVE THEORY AND TECHNIQUES and delegate in the Swedish URSI—Sections B and D.

Paper VI

"Temperature dependence and electrical properties of dominant low-frequency noise source in SiGe HBT"

S. Bruce, L. K. J. Vandamme and A. Rydberg

To be submitted.

Temperature dependence and electrical properties of dominant low-frequency noise source in SiGe HBT

S. Bruce, L. K. J. Vandamme and A. Rydberg.

Abstract

The temperature dependence and electrical properties of the dominant low-frequency noise source in a SiGe HBT has been investigated. By employing a temperature variation of the device to get a variation of the base or collector current independently of each other, it is shown that the dominant noise source is strongly dependent on the collector current, but only weakly dependent on the base current. A modified Ebers-Moll model is presented that accounts for the collector current dependence of the dominant noise source and simultaneously accounts for the temperature dependence of β. Using the modified Ebers-Moll model, the understanding of the physical positioning of the noise source is simplified.

I. Introduction

In a previously pupblished article [1] we have reported on a measurement technique for distinguishing the dominant noise source for a SiGe HBT. From the used model, it was found that the dominant noise source was located in the base-emitter junction of the device. Employing the same technique as in [1] on SiGe HBTs from providers different from the ones providing the samples in [1] it has been found that the same source has been dominant in all different samples measured so far. In a schematic small signal model of the HBT, see Fig. 1, the source is called S_{I_B} and is found to be situated in the base-emitter junction. This dominant $1/f$ source of the HBT is usually defined as:

$$S_{I_B} = S_{I_B}(f, I_B, T) \propto \frac{I_B^\delta}{f^\gamma} F(T) \tag{1}$$

where it specifically assumes a base current dependence with $1 \leq \delta \leq 2$ and a frequency dependence with $0.8 \leq \gamma \leq 1.2$. The current work is a continuation of the previous work presented in [1] and aims at further studying this source, its current and temperature dependence using the thermal behaviour of HBTs and to investigate the strict base current dependence of the source.

II. Theory

In order to study the dependence of S_{I_B} on both I_B and I_C, it is necessary to be able to vary the base current amplification factor ($\beta = I_C/I_B$). In box-shaped alloy base HBTs the electrical junction between the base and emitter exhibits a bandgap difference which ideally translates to a temperature dependence of β as:

$$\beta = K e^{\frac{L}{T}} \tag{2}$$

where K and L are constants depending on the material combination and technology of the device. Second order effects on the temperature dependence exist (e.g. bandspikes in an AlGaAs/GaAs HBT), but of main importance here is that the relation between base and collector current vary with temperature in a distinct way.

Given the temperature dependence of β, it is thus possible to vary the relation between I_B and I_C while indeed keeping one of them constant. For a typical $Si_{1-x}Ge_x$ base device having $x \approx 0.2$ the β can vary almost a factor of 2 for a temperature variation from $20°C$ to $80°C$, see Fig. 2. In doing so, either I_B or I_C can be held constant while varying the other current. In this way an explicit dependence of a dominant noise source on either I_B or I_C can be investigated.

A temperature dependence of the noise source as indicated in eq. 1, can not be excluded, but need not be detrimental to the interpretation. In a first step only a current dependence as a trend is important to distinguish which current is dominating the dependence of the noise.

By measuring the current dependence of $S_{I_{CE}}$ at a fixed temperature, an estimate of the dependence on the total of the currents I_B and I_C can be found. As the measurement is performed at a constant device temperature, β is constant and the currents will vary equally much. Preferably, one of the currents is dominant on its influence on the noise in I_C. A clear dependence when varying only one current, which deviates from the fixed temperature case, can be used to identify a temperature dependence of the noise source.

S. Bruce and A. Rydberg are with Uppsala University, Sweden.
L. K. J. Vandamme is with Eindhoven University of Technology, The Netherlands

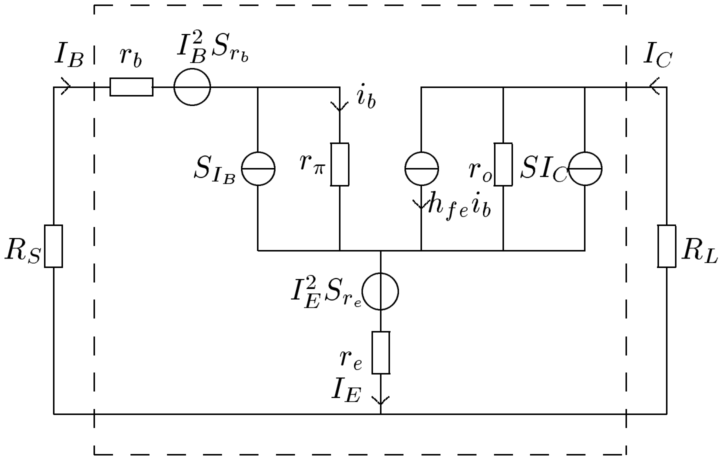

Fig. 1. Equivalent small signal circuit for an HBT in a common-emitter measurement.

III. Measurement setup

A measurement setup like the one described in [1] has been used for direct and simultaneous measurement of the current noise in the base-lead ($S_{I_{BE}}$) and in the collector-lead ($S_{I_{CE}}$). The setup enables on-wafer measurements using Ground-Signal-Ground probes and 50Ω system impedance with the possibility to insert RF-terminations at the base and collector in order to suppress oscillations.

Device temperature is controlled using a Peltier element which is actively controlled by a PID regulator. The Peltier element is heating or cooling a $2mm$ thick brass plate in which a temperature transducer (AD590) is mounted $0.5mm$ under the surface, thus giving close thermal feedback. The measured chip is fastened to the brass plate through vacuum which ensures good thermal coupling. The PID-regulator manages to maintain the temperature within $\pm 0.5°C$ from set value in the active range. Such a small and slow variation seems not to have a noticeable impact on the measured noise in the frequency range of a few Herz and on. The Peltier element is also electrically insulated from the measured device in order to minimize electrical disturbance from the necessary controller current flowing through the Peltier element.

IV. Results

In this study, SiGe devices fabricated with a technology similar to what is described in [2] and having a Germanium content of 20% in the base were used. Devices having emitter area dimensions ranging from $1.2 \times 5 \mu m^2$ to $2 \times 20 \mu m^2$ were measured. Gummel plots at device temperatures from $20°C$ to $80°C$ indicate an ideality factor close to unity at the bias point used in the noise measurements and leakage currents in the base in the lower $10nA$ range. Leakage components in the collector current were not detected. For the given temperature variation, the current amplification factor (β) was found to be 350 and 200 at $20°C$ and $80°C$ respectively. In the study, a fixed base current of $I_B = 2\mu A$ was chosen when varying the collector current by temperature and bias, and conversely collector currents of about $I_C = 0.7mA$ were chosen when varying the base current by temperature and bias. The fixed value of collector currents for the different devices were chosen as βI_B at a device temperature of $20°C$.

The noise was measured at $V_{CE} = 1.5V$ and $R_S = 50k\Omega$ (internal impedance of transimpedance amplifier and bias stage included). The frequency dependence of the noise indicates in the region below 150 Hz a true 1/f dependence. For higher frequencies, the power spectral density (PSD) suggests a Lorentzian bump in the spectrum due to generation-recombination noise. In order to minimise possible powerline interference and harmonics of 50 Hz, we choose the frequency of 74 Hz to compare experimental results. At the high value of R_S, the noise in both measurement leads is completely dominated by S_{I_B} and a full coherence is found between the two measured signals for all temperatures, see

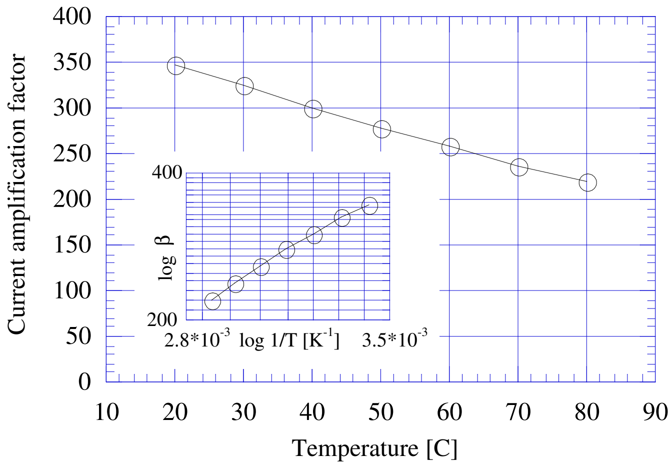

Fig. 2. Current amplification factor as a function of device temperature. The inset shows the log of the same current amplification factor versus the log of $1/T$.

Fig. 3.

A typical plot of $S_{I_{BE}}$ and $S_{I_{CE}}$ for either a variation in base current or a variation in collector current is shown in Fig. 4. By measurements as described in [1], S_{I_B} is identified as the dominant source for values of R_S above $1k\Omega$ in both measurement leads. As S_{I_B} dominates the noise in both measurement leads, it can be extracted from the measurements, considering the equivalent circuit in Fig. 1 as:

$$S_{I_B} = S_{I_{BE}} * \frac{(R_S + r_\pi)^2}{r_\pi^2} \tag{3}$$

or

$$S_{I_B} = S_{I_{CE}} * \frac{(R_S + r_\pi)^2}{\beta^2 R_S^2} \tag{4}$$

where it has been assumed that $h_{fe} \approx \beta$ which is correct since the ideality factors for both currents, in a Gummel plot, are equal and in this case very close to unity. Here r_b and $(1 + h_{fe})r_e$ are negligible in comparison with R_S and r_π. The extracted S_{I_B} using both eq. 3 and 4 are also included in Fig. 4. As the two extracted sets of S_{I_B}, for both current variations, coincide in the graph, this is a good indication that the applied extraction gives a valid result for the used model under the given bias conditions.

By comparing the straight lines indicating slopes and the extracted data for S_{I_B} in Fig. 4, a quadratic dependence on collector current is estimated. The base current dependence of S_{I_B} is very weak and no specific slope, differing from an independence of I_B, can be distinguished. From this we conclude that S_{I_B} is mainly dependent on I_C and extremely weakly dependent on I_B. The variation in base current is proportionally related to a variation in device temperature as can be found from Fig. 2, keeping in mind that the collector current is kept constant. From the weak base current dependence on S_{I_B} we thus conclude also an extremely weak thermal dependence of S_{I_B}

The main dependence of S_{I_B} on I_C indicates that the noise is dominated by an electron current since this is the only type of carriers that is swept through the collector, thus completely dominating the collector current. The very low leakage in the collector current manifested as an ideality factor being very close to unity for several decades of current indicate a very weak impact of leakage currents. From this information we conclude that the noise should be originating within the intrinsic part of the device, i.e., in the path of the electron flow.

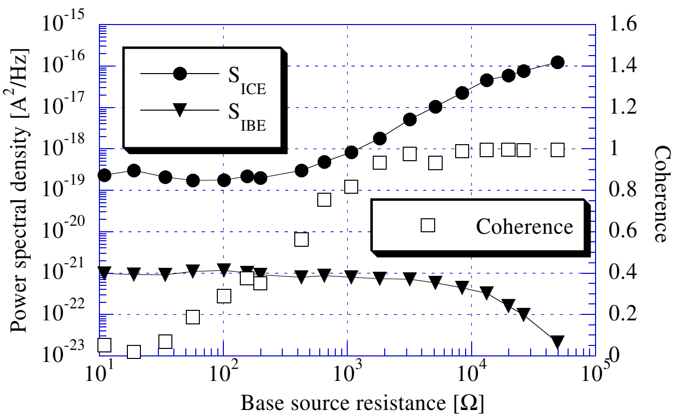

Fig. 3. Current power spectral density and coherence between the two signals for a variation in R_S.

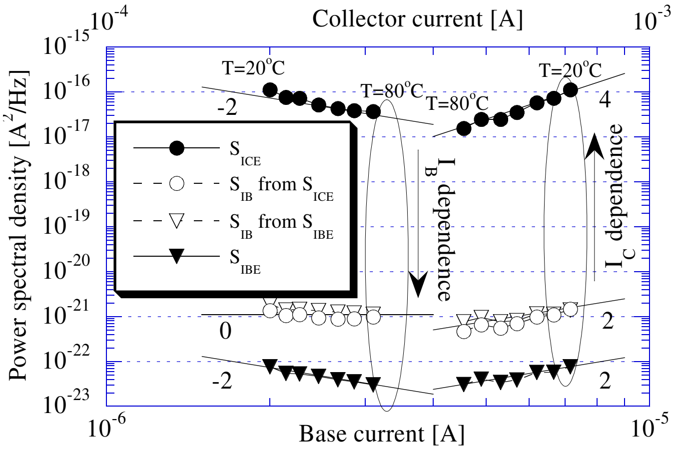

Fig. 4. Current power spectral density for a variation of I_B and I_C, $R_S = 50k\Omega$. The numbers under the straight lines indicate slopes as $y = x^n$ where n is the given number. Device temperatures are indicated for the two sets of current sweeps.

V. New model

With the results pointing out that S_{I_B} is mainly dependent on I_C, a different model which more correctly reflects the physical and electrical properties of the HBT should be employed. Based on a modified Ebers-Moll model which accounts for electron and hole injection separately [3] a small signal equivalent circuit is shown in Fig. 5. From the figure it is clear that S_{I_B} can be related to the collector current which essentially is equal to the electron current injected from the emitter into the base and further swept through the collector. As is seen in Fig. 5, the noise source is composed of noise originating from the currents flowing through both diodes (electrons and holes, respectively) shown as the current generators ΔI_h and ΔI_e respectively. Only the currents related to electrons that are swept through the collector, have corresponding current generators in the base-collector, shown as $\alpha\Delta I_e$ and αi_e. It has been assumed that the small signal base transport factor (here called α') $\approx \alpha$ and that all electrons not recombining in the base with holes are swept through the collector. Thus there should not exist any electron current generator in the base-emitter lead related to the collector current, which is without a corresponding current generator in the base-collector junction.

If, however, such a current would exist in the base-emitter junction, it could be included in ΔI_h which then would include an electron current dependence and consequently a collector current dependence.

The conductances g_h and g_e in the small signal model accounts for the dynamic conductance related to the hole and electron injection respectively.

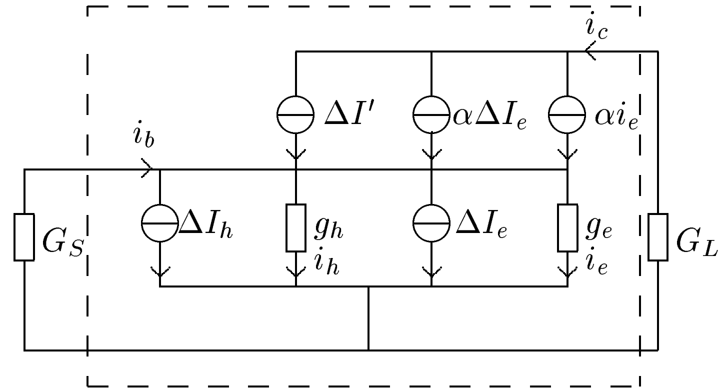

Fig. 5. Suggested new small signal model accounting for collector current dependence of dominant current noise source S_{I_B}.

In the large-signal case, the base current amplification factor β has been partitioned into two more physically related parameters: the electron injection efficiency $\gamma = I_e/I_h$, where I_e and I_h are the large signal equivalents of i_e and i_h respectively, and the base transport factor α. The electron injection efficiency, γ, can intuitively be seen as a relation between the useful electron current which to a great extent will be transported through the base and the sacrificial hole current which is necessary to maintain the base-emitter voltage drop. The parameters are related through (similar to e.g. [4]):

$$\beta = \frac{\alpha\gamma}{1+\gamma(1-\alpha)} \tag{5}$$

Similar expressions for β can be found for the small signal case giving that $h_{fe} \approx \beta$ as before. The small signal base transport factor, α', can also be assumed a value close to unity. A base transport factor close to unity and ideality factors of I_e and I_h close to unity have been assumed. The very thin base layer necessary for a strained SiGe base in combination with the measured gummel plots supports these assumptions.

Using the representation in eq. 5, the temperature dependence of β can be directly related to the bandgap difference between emitter and base. Due to the different bandgaps in the emitter and base, the hole and electron injection currents will have different temperature dependencies. Hence the electron injection efficiency, γ, will be directly affected which is reflected in β.

With the presented model, a more direct physical explanation to noise ascribed to a variation in β can be given. A variation in the injections of holes and electrons will cause the base and collector current to vary in a distinct way which is artificially related to a variation in γ and consequently a variation in β. With the word artificially we mean that a variation in γ is not a source of noise, but indicates a way of defining noise. Variations in the electron injection will thus be interpreted as a variation in β which causes a variation in I_C, using the earlier model, whereas a variation in the hole current will be interpreted as a variation in the base current. A correlation in the noise between the collector and base current may also occur due to a non-ideal base transport factor.

Noise due to a variation in the base transport factor caused by the base recombination will not be contributing to the $1/f$noise as the time constant for such process is very low and will thus give a very low noise level with a Lorentzian spectrum.

VI. Hypothesis for the origin of the source

From the new equivalent circuit, contributing sources to the noise that are physically related can be identified. In the case of an HBT, fluctuations in the current can be expected at the interfaces of the emitter-base and the base-collector respectively. As described in [5], heterojunctions with bandgap discontinuities and lattice mismatch in the interfaces will induce additional noise. A more thorough investigation of this noise source is however not the intent of this work and it suffices to notice that the noise induced at the emitter-base interface can be considered as a part of ΔI_e for the electron current and as part of ΔI_h for the hole current. The noise at the interface at the base-collector can be considered as a part of $\Delta I'$, see Fig. 5.

In addition to the sources in the base-emitter region, also a noise source in the base-collector junction (included as part of $\Delta I'$) can contribute to the noise in both the base and collector lead.

From the equivalent circuit in Fig. 5, expressions for the fluctuating currents and thus also the PSDs in the base and collector leads are derived in appendix and are found to be:

$$i_b = \frac{G_S}{G_S + g_h + (1-\alpha)g_e}\left[\Delta I' - \Delta I_h - (1-\alpha)\Delta I_e\right] \tag{6}$$

and

$$i_c = \frac{1}{G_S + g_h + (1-\alpha)g_e}\left[(G_S + g_h + g_e)\Delta I' - g_e\alpha\Delta I_h + \alpha(G_S + g_h)\Delta I_e\right] \tag{7}$$

which gives the PSDs (derived in appendix):

$$S_{I_{BE}} = \left(\frac{G_S}{G_S + g_h + (1-\alpha)g_e}\right)^2\left[S_{I'} + S_{I_h} + (1-\alpha)^2 S_{I_e}\right] \tag{8}$$

$$S_{I_{CE}} = \left(\frac{1}{G_S + g_h + (1-\alpha)g_e}\right)^2\left[(G_S + g_h + g_e)^2 S_{I'} + g_e^2\alpha^2 S_{I_h} + \alpha^2(G_S + g_h)^2 S_{I_e}\right] \tag{9}$$

From the measurements and using eq. 8 and 9, the dominant noise source is found to be either in the emitter or in the collector. From the indicated slopes in the graph of Fig. 4 a current dependence of $S_{I_{BE}}$ and $S_{I_{CE}}$ on I_B and I_C as $S_{I_{BE}} \propto I_B^{-2}$, $S_{I_{CE}} \propto I_B^{-2}$, $S_{I_{BE}} \propto I_C^2$ and $S_{I_{CE}} \propto I_C^4$ is found. To identify which source follows this dependence in eq. 8 and 9 we first observe that $g_h = I_h/v_T$ and $g_e = I_e/v_T$ and that there can only be one noise source dominant in both measurement leads since the measured coherence is very close to unity. Two noise sources can give an I_C^2 dependence in eq. 8 and at the same time give I_C^4 dependence in eq. 9. This is S_{I_h} and $S_{I'}$. The noise from S_{I_h} is by definition not related to the collector current as it indicates the hole current injected into the emitter and can thus not be the dominant source. Any inclusion of electron current dependence in S_{I_h} would however make this source a possible candidate as it then would have a collector current dependence. Investigating the existence or absence of such a dependence for S_{I_h} is however beyond the scope of this work and we observe that the analysis is valid for both sources as the factors in front of S_{I_h} and $S_{I'}$ in eq. 8 and 9 show the same dependence on base and collector current as long as $g_e \gg g_h$. Setting the external source conductance, g_h, to a high value does not simplify the interpretation for eq. 8 as base and emitter resistances not included here will limit its impact [1].

The noise from S_{I_e} shows the same collector current dependence on its multiplying factors in eq. 8 and 9 and it can for this reason not be the dominant source.

Observing the base current dependence of $S_{I_{BE}}$ and $S_{I_{CE}}$ in Fig. 4 verifies the conclusion and indicates also that $g_h > (1-\alpha)g_e$ which gives that $\alpha > \frac{\gamma-1}{\gamma}$. Noticing that γ in itself must have a greater value than the directly measurable β we find from the measurements that $\alpha \geq 0.997$ for the studied device. This verifies the assumption for α being close to unity.

In order to verify the derived location of the dominant source, the extraction shown in eq. 3 and eq. 4 must still be valid. With the already established lower limit for α, eq. 5 can be simplified to $\beta \approx \gamma$ and eq. 8 and eq. 9 simplifies to (accounting only for $S_{I'}$, the identical procedure can be performed for S_{I_h}):

$$S'_{I_{BE}} \approx \left(\frac{\frac{1}{R_S}}{\frac{1}{R_S} + \frac{1}{r_\pi}} \right)^2 S_{I'} \tag{10}$$

and

$$S'_{I_{CE}} \approx \left(\frac{1}{\frac{1}{R_S} + \frac{1}{r_\pi}} \right)^2 \left(\frac{\beta}{r_\pi} \right)^2 S_{I'} \tag{11}$$

where $R_S = 1/G_S$, $r_\pi \approx 1/g_h$ and γ has been substituted for β. Applying eq. 3 on eq. 10 or eq. 4 on eq. 11 immediately gives $S_{I_B} = S_{I'}$ as expected. Using the identical procedure for S_{I_h} will give $S_{I_B} = S_{I_h}$.

VII. Conclusion

The dominant current noise source observed in SiGe HBTs has been investigated using a temperature variation of the device. It has been observed that the previously defined S_{I_B} is mainly dependent on the collector current and that its dependence on base current is negligible. Observing an ideality factor close to unity for the collector current and observing the noise analysis in terms of full coherence between $S_{I_{BE}}$ and $S_{I_{CE}}$ indicates that the noise source should be positioned within the intrinsic part of the device, i.e., in the path of the electron flow.

A modified Ebers-Moll model where electron and hole currents are modeled separately has been introduced for the noise analysis. It gives a good description of the physical position of the noise sources. With the new model, the introduction of a noise source in the base-collector junction has been possible in a natural way. With the previously used hybrid-π model, employing its usual set of noise sources, the noise in the base-collector junction is screened from the base as this source is included in the noise source connected between the collector and emitter. The observation of such a source is thus obscured which indicates a drawback with the hybrid-π model in comparison with the now suggested model when investigating optional noise sources within the intrinsic part of a BJT. A more complex hybrid-π model may resolve the issue of including the base-collector noise source, but will still not address the collector current dependence.

From the analysis, the position of the dominant noise source can not be discriminated with full certainty as to whether it is in the base-emitter junction or in the base-collector junction. The dominant noise source is found to be temperature independent throughout the measurement range employed and to have a quadratic dependence on the collector current.

In the current work, the collector current dependence of the dominant noise source, rather than a base current dependence, is equivalent to a more commonly used base current dependence in a situation with a constant β. The collector current dependence stresses the fact that the dominant noise source is not immediately related to the base side of the transistor and then amplified through β to the collector side.

Appendix

Derivation of noise at terminals using new small signal model

In this appendix, expressions for the terminal currents into the base and collector, shown as i_b and i_c in Fig. 5 will be derived. Using these expressions, the PSDs for the current fluctuations are derived.

With Kirchoffs law, define i_b and i_c as:

$$i_b + \Delta I' + \alpha \Delta I_e + \alpha i_e - \Delta I_h - i_h - \Delta I_e - i_e = 0 \tag{12}$$

$$i_c - \Delta I' - \alpha \Delta I_e - \alpha i_e = 0 \tag{13}$$

Finding expression for i_e and i_h as dependent only on internal current sources:

$$i_e = \frac{g_e}{G_S + g_h + g_e} \left[\Delta I' - \Delta I_h - (1-\alpha)\Delta I_e + \alpha i_e \right] \tag{14}$$

$$i_h = \frac{g_h}{G_S + g_h + g_e} \left[\Delta I' - \Delta I_h - (1-\alpha)\Delta I_e + \alpha i_e \right] \tag{15}$$

Eliminating components of i_e from the right hand side in eq.14 gives:

$$i_e = \frac{g_e}{G_S + g_h + (1-\alpha) g_e} \left[\Delta I' - \Delta I_h - (1-\alpha)\Delta I_e \right] \tag{16}$$

Using eq. 16, i_h is defined as:

$$i_h = \frac{g_h}{G_S + g_h + (1-\alpha)g_e}\left[\Delta I' - \Delta I_h - (1-\alpha)\Delta I_e\right] \tag{17}$$

With eq. 12, 13, 16 and 17, expressions for i_b and i_c are found as:

$$i_b = \frac{G_S}{G_S + g_h + (1-\alpha)g_e}\left[\Delta I' - \Delta I_h - (1-\alpha)\Delta I_e\right] \tag{18}$$

and

$$i_c = \frac{1}{G_S + g_h + (1-\alpha)g_e}\left[(G_S + g_h + g_e)\Delta I' - g_e\alpha\Delta I_h + \alpha(G_S + g_h)\Delta I_e\right] \tag{19}$$

The PSDs are thus found to be:

$$S_{I_{BE}} = \left(\frac{G_S}{G_S + g_h + (1-\alpha)g_e}\right)^2\left[S_{I'} + S_{I_h} + (1-\alpha)^2 S_{I_e}\right] \tag{20}$$

$$S_{I_{CE}} = \left(\frac{1}{G_S + g_h + (1-\alpha)g_e}\right)^2\left[(G_S + g_h + g_e)^2 S_{I'} + g_e^2\alpha^2 S_{I_h} + \alpha^2(G_S + g_h)^2 S_{I_e}\right] \tag{21}$$

where the use of S indicates the PSD of each individual noise source in the right hand side of eq. 20 and eq. 21. The indices I_{BE} and I_{CE} on the left hand side refers to the common-emitter base and collector current noise measurement respectively.

Acknowledgement

The authors are grateful to Uwe Erben and Andreas Schüppen, TEMIC semiconductors, Germany for useful discussions and for providing samples of HBTs for measurements. The Swedish Strategic Foundation (SSF) is acknowledged for partially funding the project through the microelectronics consortium "HF Bipolar Technology"

References

[1] S. Bruce, L. K. J. Vandamme, and A. Rydberg, "Low frequency base and collector current noise and coherence as function of bias in SiGe heterojunction bipolar transistors," *IEEE Trans. Elec. Devices*, vol. 46, pp. 993–1000, 1999.

[2] A. Schüppen, H. Dietrich, S. Gerlach, H. Höhnemann, J. Arndt, U. Seiler, R. Götzfried, U. Erben, and H. Schumacher, "SiGe-technology and components for mobile communication systems," in *Proc. 1996 BIPOLAR/BiCMOS Circuits and Technology Meeting*, 1996, pp. 130–133.

[3] S. Bruce, A. Rydberg, M. Kim, F. Beißwanger, J. F. Luy, H. Schumacher, U. Erben, M. Willander, and M. Karlsteen, "Design and realisation of a millimeter-wave Si/SiGe HBT frequency multiplier," *IEEE Trans. on Microwave Theory and Tech.*, vol. 46, no. 5, pp. 695 – 700, May 1998.

[4] H. Craig Casey, jr., *Devices for integrated circuits (Silicon and III-V Compound Semiconductors)*, chapter 9, pp. 433–445, Wiley, New York, 1999, ISBN-0- 471-17134-4.

[5] L. K. J. Vandamme, S. Kibeya, S. Orsal, and R. Alabedra, "1/f noise and thermal noise of $GaAs/Al_{0.4}Ga_{0.6}As$ superlattice," *Noise in physical systems and 1/f fluctuations*, vol. 285, pp. 324–328, 1993.

Paper VII

"Improved coherence measurements using voltage and transimpedance amplifiers in noise characterization of bipolar transistors"

S. Bruce, L. K. J. Vandamme and A. Rydberg

To be submitted.

Improved coherence measurements using voltage and transimpedance amplifiers in noise characterization of bipolar transistors

S. Bruce, L. K. J. Vandamme and A. Rydberg

Abstract

A method is presented to improve accuracy in noise characterization of bipolar transistors by using both a voltage amplifier and transimpedance amplifiers.

I. Introduction

In measurements performed using transimpedance amplifiers at both base and collector as described in [1], noise can be induced from the base-lead current amplifier into the device under test (DUT) for low base resistance terminations (R_S in Fig. 1). Its artifact results in increased collector current noise floor above what can be expected from the intrinsic device and thus the coherence between the two measured noise signals is inadvertently decreased. For characterization purposes it is important to be able to find information about the intrinsic devices, e.g., for a complete sweep of base-resistance terminations. It is also important to be able to perform correct measurements for an as wide range of circuit setups as possible.

The noisy active input of the transimpedance amplifier is here replaced with a passive input voltage amplifier.

II. Theory

A method to partly circumvent the problem of the induced voltage noise into the base is to use voltage amplifiers having a passive input. The amplifier will only induce additional noise at the output.

The measurements are performed in two steps. In the first step, the base and collector current noise ($S_{I_{BE}}$ and $S_{I_{CE}}$ respectively) are characterized using transipedance amplifiers as described in [1]. The level of $S_{I_{CE}}$ for low values of base resistance termination (R_S in Fig. 1) is then disturbed and coherence between $S_{I_{BE}}$ and $S_{I_{CE}}$ is systematically too low. In the second step, the transimpedance amplifier at the base is exchanged with a voltage amplifier, measuring the voltage noise induced over R_S, see Fig. 1. As the voltage amplifier has a passive input, the level of $S_{I_{CE}}$ is not affected for low values of R_S, but the level of $S_{I_{BE}}$ is difficult to measure accurately as the conversion into voltage noise over R_S will be low. The measurement using a voltage amplifier serves mainly to find the coherence between $S_{I_{BE}}$ and $S_{I_{CE}}$. A good agreement between measured and calculated coherence, as will be described, indicates a correct understanding of the levels of the different disturbing noise sources. Thus a good prediction of the true coherence value between $S_{I_{BE}}$ and $S_{I_{CE}}$ even at small values of R_S can be made.

The measured voltage noise, $S_{V_{BE}}$ in Fig. 1, will mainly consist of three different parts: intrinsic noise from within the transistor (the expected noise), noise from the amplifier itself ($S_{V_{amp}}$ in Fig. 1) and Nyquist noise from the base series termination (R_S in Fig. 1). The desired current noise will create a voltage noise over R_S and the total output noise ($G^2 S_{V_{BE}}$) can thus be calculated as:

$$G^2 S_{V_{BE}} = G^2 \left(S_{I_{BE}} R_S^2 + 4k_B T R_S + \frac{S_{V_{amp}}}{G^2} \right) \tag{1}$$

where G is the voltage amplification factor of the amplifier and the noise level has been calculated to the level before amplification, thus the division by G^2 of $S_{V_{amp}}$.

Assuming that only one noise source is dominant within the transistor for both the base and collector current noise [1] and that the only additional noise sources are the ones mentioned above, a value of the coherence can be calculated as:

$$\gamma^2 = \frac{S_{I_{BE}} R_S^2}{S_{I_{BE}} R_S^2 + 4k_B T R_S + \frac{S_{V_{amp}}}{G^2}} \tag{2}$$

S. Bruce and A. Rydberg (Signals and Systems, Uppsala University, P.O. Box 528, SE-751 20 Uppsala, Sweden)
L. K. J. Vandamme (Dept. Electrical Engineering E.H.5.15, Eindhoven University of Technology, 5600MB Eindhoven, The Netherlands)

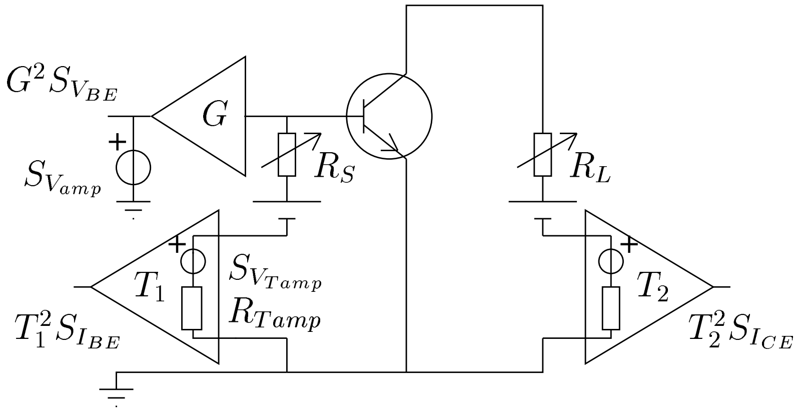

Fig. 1. Schematic circuit setup of coherence measurements using both a voltage and a transimpedance amplifier in the base-lead. The voltage noise source at the output of the voltage amplifier indicates the internal noise of the voltage amplifier.

The equivalent voltage noise level of the desired noise should thus preferably be in the same range as $S_{V_{amp}}/G^2$ or above. The value of R_S should be chosen sufficiently high that the first term on the right hand side in eq. 1 amounts to at least 1/9 of the total noise level for reasonable accuracy in detection of the coherence.

III. Measurements

To verify the described method, noise measurements on a $1.2 \times 20\mu m^2$ SiGe HBT device has been performed. Using a measurement setup shown in Fig. 1, $S_{I_{BE}}$, $S_{I_{CE}}$ and the coherence between the two signals were measured, see Fig. 2. The curves with filled symbols indicate measurements using transimpedance amplifiers at both base and collector. Curves with open symbols indicate measurements where a voltage amplifier has been used at the base, the transimpedance amplifier has then been removed. The current PSD ($S_{I_{BE}}$) in the latter setup has been calculated using eq. 1 as:

$$S_{I_{BE}} = \frac{S_{V_{BE}} - \frac{S_{V_{amp}}}{G^2} - 4k_B T R_S}{R_S^2} \tag{3}$$

The strong deviation of the calculated value of $S_{I_{BE}}$ (shown as open triangles in Fig. 2) for low values of R_S ($R_S \leq 50\Omega$) from the measured values using transimpedance amplifiers (shown as filled triangles) is explained by that the desired noise signal is far from dominating in the output signal of the voltage amplifier for these values of R_S.

From Fig. 2 (filled triangles), $S_{I_{BE}}$ is found to be $8 \cdot 10^{-22} A^2/Hz$. Measuring the output noise of a short-circuited voltage amplifier gives that $S_{V_{amp}}/G^2 \approx 1.1 \cdot 10^{-18} V^2/Hz$ and a value of $R_S \geq 38\Omega$ would thus make $S_{I_{BE}}$ dominate over $S_{V_{amp}}$ in the output signal.

In Fig. 2 it is seen that the coherence remains high for a wider range of R_S when using a voltage amplifier in comparison with using a transimpedance amplifier at the base, as expected. An expected value of the transferred noise into $S_{I_{CE}}$ when a transimpedance amplifier is connected to the base can be calculated as (for low values of R_S):

$$S_{I_{CE_{transferred}}} = S_{V_{Tamp}} \left(\frac{h_{fe}}{r_\pi} \right)^2 \tag{4}$$

where h_{fe} and r_π is the small signal current amplification factor and input base-emitter dynamic resistance, respectively, of the DUT. $S_{V_{Tamp}}$ is the output voltage noise from the input of the transimpedance amplifier into the base, see Fig. 1. From DC-characterization and calibration measurements, the current amplification factor of the device was found to be $h_{fe} \approx 280$ and $S_{V_{Tamp}} \approx 1.3 \cdot 10^{-16} V^2/Hz$ at $235Hz$. Assuming all resistance values except $r_\pi \approx 13k\Omega$ being negligible, the current PSD at the collector is found to be $S_{I_{CE}} \approx 6 \cdot 10^{-20} A^2/Hz$ which compares very well with the measured values, see Fig. 2, filled circles. When the transimpedance amplifier is exchanged for a voltage amplifier at the base, $S_{I_{CE}}$ (open circles) drops to $S_{I_{CE}} \approx 6 \cdot 10^{-21} A^2/Hz$ for low values of R_S. The same result is found when no amplifier is connected to the base (open dotted circles).

Any induced noise into the base from the measurement setup except $S_{V_{Tamp}}$ can be excluded by the fact that once induced into the base, it would give rise to the voltage noise of $S_{V_{unknown}} \approx 1.3 \cdot 10^{-17} V^2/Hz$ calculated using eq. 4 with data from $S_{I_{CE}}$ measured using the voltage amplifier at the base (open circles) for low values of R_S. This level was however not found. It is thus shown that the collector current noise PSD is originating from within the device and following the discussion in [1], circuit parameters of the DUT are possible to extract.

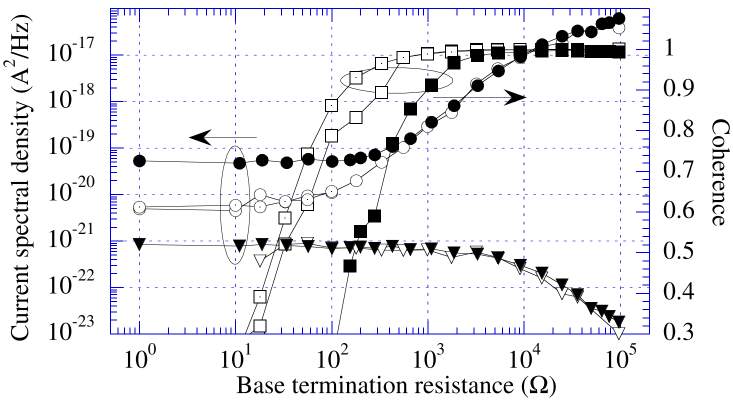

Fig. 2. Plot of $S_{I_{BE}}$, $S_{I_{CE}}$ and the coherence between the measured signals versus a base resistance termination, R_S. Device temperature is $25°C$, $I_B = 2\mu A$, $I_C = 0.56mA$ and $V_{CE} = 1.5V$. The frequency is $235Hz$. Filled symbols indicate measurements using transimpedance amplifiers at both base and collector. Open symbols indicate measurements where the base transimpedance amplifier has been substituted with a voltage amplifier.

Using eq. 2, a calculated value of the coherence for the case of a voltage amplifier at the base is found and included in the graph as dotted, open squares, see Fig. 2. The calculated value of the coherence compares very well with the measured one also for values of $R_S \leq 200\Omega$ down to values of R_S where the coherence is below detection limit. The assumption made for eq. 2 is thus likely valid and it can be concluded that a full coherence between the current noise from the base and the collector exists also for values of at least $R_S \geq 50\Omega$. For values of $R_S \leq 20\Omega$, the coherence is below detection limit and a direct conclusion should not be drawn.

However, in Fig. 2 it is seen that $S_{I_{CE}}$ reaches a constant level for values of $R_S < 100\Omega$ and from measurements using transimpedance amplifiers it is seen that $S_{I_{BE}}$ has a constant level for $R_S < 1k\Omega$. Thus, since a full coherence between the signals can be assumed for values of $R_S > 20\Omega$ it can be concluded that the coherence and the levels of the PSDs will remain also for lower values of R_S than 20Ω as both $S_{I_{BE}}$ and $S_{I_{CE}}$ appear independent on R_S for low values of the base resistance termination.

IV. Conclusion

It has been shown that by employing two different measurement strategies, the PSD of both $S_{I_{BE}}$, $S_{I_{CE}}$ and the coherence between the signals for a full range of base resistance termination, R_S, can be found. By combining information gathered from both methods, weaknesses in each of the two can be circumvented.

References

[1] S. Bruce, L. K. J. Vandamme, and A. Rydberg, "Low frequency base and collector current noise and coherence as function of bias in SiGe heterojunction bipolar transistors," *IEEE Trans. Elec. Devices*, vol. 46, pp. 993–1000, May 1999.

Paper VIII

"Simulation of noise in SPICE-like simulators using AC voltage and current sources only"

S. Bruce, L. K. J. Vandamme and A. Rydberg

To be submitted.

Simulation of noise in SPICE-like simulators using AC voltage and current sources only

S. Bruce, L. K. J. Vandamme and A. Rydberg

Abstract

A method for simulating noise sources in an arbitrary circuit where coherence and power spectral densities can be accurately calculated using regular voltage and current AC sources, is presented. The method is based on a set of simulations where the different sources are made orthogonal by shifting the phase offset by different multiples of 2π. The averaged resulting signals then correspond to the noise levels. Coherence between the different sources can also be calculated.

I. Introduction

To enable a correct simulation of low-frequency noise in an electronic circuit, it is important to be able to control the noise sources very precisely and also be able to distinguish between them in a convenient way. Regular simulators tend to treat this kind of noise only as a random signal with an arbitrary, not known, phase which is quite sufficient for simulations where the noise is not to be specifically studied. When performing simulations where coherence between studied signals are of interest, the phase-offset and the amplitude of the individual noise sources need to be known.

II. Theory

The definition of an ensemble average of a spectral density (SD) for two time dependent signals ($x(t)$ and $y(t)$) is defined as:

$$\overline{S_{xy}(\omega)} = \lim_{T\to\infty} \left\{ \frac{2\overline{X(\omega)Y^*(\omega)}}{T} \right\} \tag{1}$$

where $X(\omega)$ and $Y(\omega)$ denote the Fourier spectrums of the two time dependent signals, T is the length of the truncated time sequence and the bar indicates an ensemble average. In electronic circuits the noise processes can be considered stationary and thus an ensemble average can be considered equivalent with a time average [1]. The coherence is defined as:

$$\Gamma^2_{xy}(\omega) = \frac{\left(\overline{S_{xy}(\omega)}\right)^2}{\left(\overline{S_{xx}(\omega)S_{yy}(\omega)}\right)} \tag{2}$$

For two signals ($x(t)$ and $y(t)$) that are uncorrelated, the phase of each member of $X(\omega)$ and $Y(\omega)$ are also uncorrelated and thus the ensemble average of a product of these will cancel:

$$\overline{S_{xy}(\omega)} = 0 \tag{3}$$

From eq. 1 it is seen that an ensemble average of a SD of a single signal will be real and non-negative:

$$\overline{S_{xx}(\omega)} = |\overline{S_{xx}(\omega)}| \tag{4}$$

To implement the noise simulation in a regular SPICE-like simulator, the approach is to use the small-signal AC simulation where the noise sources are defined as regular independent voltage and current sources in the frequency domain.

The phase offset of the different sources are varied independently of each other. By averaging the results from a set of simulations, eq. 3 will be satisfied, i.e.:

$$\sum_{k=1}^{2N} X_{n_k}(\omega)X^*_{m_k}(\omega) = 0, \qquad m \neq n \tag{5}$$

S. Bruce and A. Rydberg (Signals and Systems, Uppsala University, P.O. Box 528, SE-751 20 Uppsala, Sweden)
L. K. J. Vandamme (Dept. Electrical Engineering E.H.5.15, Eindhoven University of Technology, 5600MB Eindhoven, The Netherlands)

and in a similar way to satisfy eq. 4:

$$\frac{1}{2N}\sum_{k=1}^{2N} X_{n_k}(\omega)X^*_{n_k}(\omega) = |\overline{X_n(\omega)}|^2 \tag{6}$$

where $X_n(\omega)$ and $X_m(\omega)$ are the new frequency domain functions. The indices m and n denote the process, previously indexed x and y. The function that has been chosen here is:

$$X_{n_k}(\omega) = |\overline{X_n(\omega)}|e^{\frac{j2\pi nk}{2N}}, \qquad\qquad 0 \le n \le N \tag{7}$$

In a practical situation, a set of $2N$ simulations of the same circuit need to be run in order to satisfy eq. 5. Thus for a circuit with K independent noise sources, one choose $N = K - 1$.

III. The circuit setup, simulation procedure and treatment of resulting data

The method was evaluated using MDS [2], a simulation package from HP with a graphical interface. Some control elements, enabling a set of simulations to be made at one instance, are specific for the package, but the implementation is still of general nature; the same procedure should be possible to repeat with any SPICE-like simulator.

As described in the previous section, a set of independent AC signal sources are used. They can be either of voltage or current type. The amplitude of the signal of each source is entered as (see Fig. 1):

$$\texttt{An= sqrt(Sn/2)} \tag{8}$$

and the phase offset of each source as:

$$\texttt{PHn=n*W} \tag{9}$$

where `Sn` is the PSD of a given noise source and n is the index ($n = 0..K-1$) for the specific source. `W` is defined as:

$$\texttt{W = 360 * k/(2 * N)} \tag{10}$$

with `k = 1..2N`.

After the simulations have been performed, SDs and coherence are calculated as a summation of complex phasors (compare with eq. 1 and 2):

$$\texttt{Smn= sum(2 * Vm*conj(Vn))/(2 * N)} \tag{11}$$

and

$$\texttt{COHmn= mag(Smn/(sqrt(Smm * Snn)))} \tag{12}$$

where m and n denote the different signals.

IV. Verification

In MDS, an arbitrary set of simulations can be performed through the `*CONTROLLER*`, `STIMULUS` and `*AC SIMULATION*` elements (see Fig. 1), thus enabling sweeps of circuit parameters in the same run as the different phase-offsets of the sources are swept. A typical, though simple, circuit is shown in Fig. 1 where three independent noise sources are implemented (called `SRC0`, `SRC1` and `SRC2` in Fig. 1). The simulation will sweep the power level for the different sources through `S_in` using the `PowerSweep` and `PowerStimulus` control blocks. For each power level, the variable `n` will be swept for the variation in phase offset (`PH0`, `PH1` and `PH2`) using the `ACsimulation` and `ACStimulus` simulation blocks. The underscore character used in the names of different variables (e.g. "`S_in`") in Fig. 1 and 2 has no significance and is only inserted to avoid conflicts with reserved names within MDS. Also, MDS uses degrees instead of radians which is seen in the definition of `W`.

As the circuit is set up, the output SD at the nodes `V1` and `V1` will remain constant, but the coherence will go from 0 (when the two measured nodes `V1` and `V2` have no signal in common, i.e., when the source in the center of the circuit is not contributing at all) to 1 (when only the source in the center of the circuit contributes).

The output from the simulation is shown in Fig. 2 and the result is in agreement with theory. The reason for the two step summation and the use of the `real` and `imag` functions are due to the difficulties for MDS to handle complex numbers when doing summations.

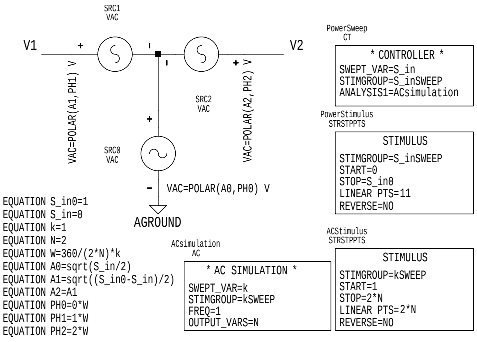

Fig. 1. Example of circuit with voltage sources representing noise sources.

```
S_11s=2*V1*conj(V1)/(2*N)      S_11=sum(real(S_11s))
S_22s=2*V2*conj(V2)/(2*N)      S_22=sum(real(S_22s))
S_12s=2*V1*conj(V2)/(2*N)      S_12=complex(sum(real(S_12s)),sum(imag(S_12s)))
                               COH=mag(S_12^2/sqrt((S_11*S_22)))
```

S_11	s_22	s_12	COH
1.000	1.000	-13.48E-15+j13.4E-15	362.5E-30
1.000	1.000	0.10+j16.1E-15	0.010
1.000	1.000	0.20+j16.1E-15	0.040
1.000	1.000	0.30+j15.5E-15	0.090
1.000	1.000	0.40+j14.6E-15	0.160
1.000	1.000	0.50+j13.4E-15	0.250
1.000	1.000	0.60+j11.9E-15	0.360
1.000	1.000	0.70+j10.1E-15	0.490
1.000	1.000	0.80+j8.0E-15	0.640
1.000	1.000	0.90+j5.3E-15	0.810
1.000	1.000	1.00+j0.00	1.000

Fig. 2. Resulting output from an MDS simulation with the circuit in Fig. 1. Very small numbers (e.g., 362.5E − 30 in the first row of the COH column) can be seen as equivalent to 0, but are retained as it is the original output from the simulator

V. Conclusions

A simple method for simulating uncorrelated noise sources using regular AC simulation in a SPICE like simulator is presented. The number of simulations that is necessary to acquire a correct result is directly proportional to the number of uncorrelated sources. The method can be used for studying the impact from a variation of circuit parameters on the noise at a given frequency.

References

[1] M. J. Buckingham, *Noise in electronic devices and systems*, Ellis Horwood Ltd., 1983.
[2] Hewlett Packard corp., Santa Rosa, Calif. U.S.A., *Microwave Design System*.